Jag1 coordinates release from multipotency with cell fate choice in the developing pancreas

by

Philip A. Seymour[1†], Caitlin A. Collin[1†§], Mette C. Jørgensen[1], Itaru Imayoshi[2], Kristian H. de Lichtenberg[1], Raphael Kopan[3], Ryoichiro Kageyama[2] and Palle Serup[1*]

[1]The Novo Nordisk Foundation Center for Stem Cell Biology (DanStem), University of Copenhagen, Blegdamsvej 3B, DK-2200, Copenhagen N, Denmark.

[2]Institute for Frontier Life and Medical Sciences, Kyoto University, Kyoto, 606-8507, Japan.

[3]Division of Developmental Biology, Cincinnati Children's Hospital Medical Center, Cincinnati, OH 45229, USA.

[†]P.A.S. and C.A.C. are shared first authors.

[§]Present address: Ocular Genomics Institute, Massachusetts Eye and Ear, Harvard Medical School, Boston, MA 02114, USA.

[*]Corresponding author:

Address: NNF Center for Stem Cell Biology

Panum Institute

Blegdamsvej 3B

Building 6.4.22

DK-2200 Copenhagen, Denmark

E-mail: palle.serup@sund.ku.dk

Abstract

Notch signaling governs the proliferation of multipotent pancreatic progenitor cells (MPCs) and their segregation into proximal duct/endocrine bipotent progenitors (BPs), and distal unipotent pro-acinar cells (PACs). However, it is unclear which ligands are involved and when they act. Here we show antagonistic effects of Jag1 and Dll1 on MPC proliferation. Furthermore, blocking Notch signaling before E13 shunts MPCs into the distal PAC fate, while later inactivation shunts BPs to endocrine differentiation. All BPs are eliminated in *Jag1*, *Dll1* double mutants, with Jag1 expression in PACs proving critical for specification all but the most proximal 5% of BPs. Hes1 expression is elevated in E12.5 *Jag1* mutant pancreas and release from the multipotent state is delayed. However, by E14.5 Hes1 expression becomes attenuated, coincident with the biased adoption of a PAC fate. Remarkably, ductal morphogenesis and organ architecture are minimally perturbed in the absence of *Jag1* until later stages, when ductal remodeling fails and signs of acinar-to-ductal metaplasia appear. Our study uncovers that an interplay between Jag1 and Dll1 control the multipotent state and that they together specify the entire pancreatic duct cell lineage.

Deciphering the mechanisms that control the differentiation of progenitor cells into one of several possible cell fates is crucial for understanding disease etiology and for using pluripotent stem cells in cell replacement therapy applications. The three principal cell lineages of the mammalian pancreas, acinar, duct and endocrine, arise from multipotent pancreatic progenitor cells (MPCs) through a series of binary cell fate choices[1]. MPCs are specified from the posterior foregut endoderm as dorsal and ventral anlagen at around embryonic day (E)8.5[2], and are distinguished by their expression of several transcription factors including Pdx1, Ptf1a, Hnf1β, Sox9 and Nkx6-1. The multipotentiality of these cells has been demonstrated at the population level by many lineage-tracing studies[3-7] and, more recently, at the clonal level[8].

The dorsal MPCs give rise to an early wave of endocrine cells from ~E9.5 to ~E11 while endocrinogenesis is delayed ~36 hours in the ventral anlage[9-11]. The appearance of hormone-producing cells is preceded by, and dependent on, expression of *Neurog3* (encoding Ngn3) in endocrine precursors, which initiates at E8.5 in the dorsal bud and E10.0 in the ventral bud[3,12,13]. Intriguingly, there is a transient decline in *Neurog3* expression from E11 to E12[12] commensurate with the segregation of Ptf1a^{+}Nkx6-1^{+} MPCs into proximal, Ptf1a^{-}Nkx6-1^{+} bipotent progenitors (BPs) and distal, Ptf1a^{+}Nkx6-1^{-} pro-acinar cells (PACs)[14,15]. This proximodistal (PD) patterning is regulated by Notch signaling. For example, forced expression of a Notch intracellular domain (NICD) prevents MPCs from adopting a PAC fate[15-17] while dominant-negative Maml1 prevents a BP fate[18,19]. Total inactivation of Notch signaling in the endoderm, as seen in *Foxa2*$^{T2AiCre/+}$; *Mib1*$^{f/f}$ (*Mib1*$^{\Delta Foxa2}$) embryos, results in a complete shift from BP- to PAC fate[19]. Downstream of Notch, PD patterning depends on mutually antagonistic interactions between Ptf1a and Nkx6-1/Nkx6-2[15].

Notch signaling, and its downstream target gene *Hes1*, have previously been shown to prevent precocious and excessive endocrine differentiation[20,21], and independently of this also stimulate MPC proliferation[22]. After PD patterning is complete at around E14, Notch signaling and Hes1 expression persist in BPs where they maintain Sox9 expression and ductal fate, and inhibit endocrine differentiation by repressing *Neurog3*[23-27]. Less is known about which ligands regulate the adoption of distinct cell fates. Dll1 is involved in the control of early endocrine differentiation[20,22]. Yet, PD patterning is unaffected in *Dll1*$^{\Delta Foxa2}$ embryos[19] and the endocrinogenic phenotype of

E10.5 *Dll1*$^{\Delta Foxa2}$ embryos is much weaker than that of E10.5 *Mib1*$^{\Delta Foxa2}$ embryos, in which essentially the entire dorsal bud is converted into glucagon cells[19,28]. Together, these findings show that additional Mib1 substrates, most likely other Notch ligands, are involved in these cell fate decisions. In zebrafish, intrapancreatic duct cells are depleted in *jag1b*/*jag2b* morphants[29,30] and completely absent from *jag1b*$^{-/-}$*; jag2b*$^{-/-}$ embryos[31] with the latter also showing a reduction in endocrine cells while acinar cells were unaffected. However, in mice Jag1 is the only Jagged-type ligand expressed in the pancreatic endoderm[32], and while conditional deletion of *Jag1* using *Pdx1*-Cre causes ductal malformation and ductal paucity postnatally, this was attributed to reduced duct cell proliferation[33]. Recently, conditional double-deletion of Dll1 and Jag1 with *Ptf1a*^{Cre} was shown to yield a relatively modest phenotype with loss of only the terminal duct or centroacinar cells (CACs)[34]. Thus, which ligands regulate the various cell fate decisions during mammalian pancreatic development remain unclear and the time when Notch signaling transitions from regulating PD patterning to controlling duct-endocrine fate choice remains undefined.

In this study, we demonstrate that Jag1 is crucial for segregation of MPCs into the BP and PAC lineages of the secondary transition pancreas. We show that down-regulation of Notch activity and resolution of the MPC markers Nkx6-1, Ptf1a, and Sox9 into their distinct BP and PAC compartments is delayed by two days in *Jag1*$^{\Delta Foxa2}$ embryos. During the eventual segregation around E14.5 – E15.5, most of the prospective BPs are mis-specified into PACs such that Ptf1a^{+} PACs entirely replace the Sox9^{+}Nkx6-1^{+} BPs normally found in the branches of the epithelial tree. The few remaining BPs, located in the central core of the organ, depend on Dll1 function as they are lost in *Dll1; Jag1*$^{\Delta Foxa2}$ embryos, resulting in a pancreas essentially comprising acinar cells only. Remarkably, epithelial plexus formation and the gross architecture of the organ are remarkably unperturbed in spite of the profound changes in cell fate. However, at late stages larger ducts are missing or malformed, terminal ducts are morphologically abnormal and signs of acinar-to-ductal metaplasia (ADM) appear. Thus, cell fate allocation and organ architecture are achieved *via* independent pathways during mammalian pancreas morphogenesis.

Results

Jag1 expression marks nascent PACs. Since BPs are converted to PACs in *Mib1*$^{\Delta Foxa2}$ embryos, but not in *Dll1*$^{\Delta Foxa2}$ embryos[19], we reasoned that an additional Mib1 substrate, most likely Jag1[20,22,32,34-36], must act during PD patterning. Because the reported expression patterns are not entirely consistent, we decided to re-analyze the expression of these two ligands by targeting fluorescent protein reporters to the *Dll1* and *Jag1* loci. The resulting *Jag1*^{J1VmC} and *Dll1*^{D1VmC} alleles comprise a Venus-T2A-mCherry cassette inserted in frame with the coding region of the last exons to generate Dll1- and Jag1-Venus fusion proteins that serve as dynamic reporters of ligand protein expression while mCherry acts as a more sensitive reporter owing to its longer half-life and as a consequence of being cleaved from the fusion protein (Supplementary Fig. 1). Co-immunofluorescence (IF) analysis with anti-RFP antibodies did not detect mCherry prior to E10.5 in *Jag1*$^{J1VmC/+}$ pancreas, at which stage it was seen in most Pdx1^{+}Sox9^{+} MPCs and in the surrounding mesenchyme. At E11.5 mCherry expression appeared intensified in the distal epithelium, and by E12.5 expression was largely confined to distal cells and extinguished from many proximal Sox9^{+} emerging BPs. By E15.5 mCherry was prominently expressed in vascular cells and very weakly in acinar cells but, in spite of previous reports[34,35], it was not detectable in Sox9^{+} BPs of the ducts (Supplementary Fig. 1). Anti-GFP antibodies reproduced the uniform expression pattern for the Jag1-Venus fusion protein in E10.5 *Jag1*$^{J1VmC/+}$ dorsal pancreas epithelium and surrounding mesenchyme (Fig. 1b) and the restriction to the distal epithelium at E12.5, with most of the centrally located Sox9^{+} emerging BPs being negative for Jag1-Venus (Fig. 1c). At E15.5, weak Jag1-Venus expression was detected apically in acinar cells and in non-parenchymal cells, including the vasculature, but expression was excluded from Sox9^{+} BPs (Fig. 1d). Since the Jag1 expression pattern we observe conflicts with previous work[34,35], we validated two anti-Jag1 antibodies (see Methods). Both reproduced the Jag1-reporter expression pattern in wild type pancreas, and IF analysis for additional markers revealed expression in vascular cells and a very low level in acinar cells at E15.5, its absence from Sox9^{+} BPs at the later stages and from the endocrine lineage at all stages (Supplementary Fig. 2).

In *Dll1*^{D1VmC} embryos anti-RFP antibodies detected scattered mCherry^{+} cells in E9.5 dorsal pancreas which were often also Sox9$^{Lo/-}$ and located adjacent to Sox9^{+}mCherry$^{Lo/-}$ cells. A similar pattern of mCherry expression was seen at E10.5, E11.5 and E12.5, with the mCherry^{+} cells frequently seen in small clusters of 2-5 cells. At E15.5, many mCherry^{+} cells were found in forming acini, often interspersed with mCherry^{-} cells (Supplementary Fig. 1). Anti-GFP antibodies reproduced this pattern with detection of Dll1-Venus fusion protein in dispersed cells throughout the E10.5 and E12.5 dorsal pancreatic epithelium, many of which were Sox9$^{Lo/-}$ (Fig. 1h,i). By E15.5, Dll1-Venus was found intracellularly in the apical pole of acinar cells, and in scattered Sox9$^{Lo/-}$ cells in the proximal epithelium that most likely represent endocrine precursors (Fig. 1j). A validated anti-Dll1 antibody reproduced this expression pattern in wild type tissue; co-staining for lineage markers showed that Dll1^{+} cells could be subdivided into several populations comprising Dll1^{+}Ptf1a^{+} MPCs or PACs present in E10.5, E12.5, and E15.5 pancreas epithelium as well as Dll1^{+}Ngn3^{+} endocrine precursors, evident at all stages, and Dll1^{+}Ngn3^{-} cells in E12.5 proximal epithelium (Supplementary Fig. 2). Co-expression of Dll1 and Jag1 was evident in E10.5 Sox9^{+} MPCs (Fig. 1e,k) and in a subset of distal cells at E12.5 (Fig. 1f,l). IF for Jag1, Dll1, Ptf1a and Nkx6-1 revealed that these were Ptf1a^{+} and Nkx6-1^{-} or Nkx6-1^{Lo}, likely representing nascent PACs and MPCs, respectively (Fig. 1o-y). The few Nkx6-1^{Hi} cells found in the distal epithelium were typically Jag1$^{Lo/-}$Dll1^{-}Ptf1a^{-} (Fig. 1n-s). Conversely, in the Ptf1a^{-} proximal region Dll1^{+} cells were Jag1^{-} and either Nkx6-1^{+} or Nkx6-1^{-} (Fig. 1t-y), which may represent either BPs or endocrine precursors derived from BPs.

Notch activity is suppressed in nascent PACs. To define the cells in which Notch receptors have been activated before and during PD patterning we first analyzed embryonic pancreata from the Notch1 activity-trap mouse line N1IP::Cre^{HI}; *Rosa26*$^{LSL\text{-}Ai3}$ in which EYFP permanently labels the progeny of cells experiencing Notch1 activation (Fig. 2a)[37]. We detected YFP labeling in a few E10.5 Ptf1a^{+}Sox9^{+} MPCs and at E12.5 we found YFP expression in Ptf1a^{+} nascent PACs, Sox9^{+} nascent BPs and in Ptf1a^{+}Sox9^{+} MPCs (Fig. 2b,c). Quantification revealed that YFP^{+} cell distribution reflected no bias towards either nascent BPs or PACs at E12.5 (Fig 2d), consistent with the cells experiencing Notch1 activation in MPCs, from which both lineages derive,

prior to the linage segregation occurring by E12.5. Since this reporter is specific to Notch1, we next analyzed Hes1 expression as a general, pan-Notch acute readout. We bred mice harboring the *Hes1*-EGFP reporter[24] to the *Jag1*^{J1VmC} and *Dll1*^{D1VmC} lines and assayed for EGFP expression using an antibody that only detects the high levels of (cytoplasmic) EGFP derived from the *Hes1*-EGFP reporter, but not the low levels of (membrane-associated) Jag1-Venus or Dll1-Venus fusion proteins (Fig. 2e-n). We compared expression of EGFP to that of mCherry and Sox9 by IF. EGFP^{+}Sox9^{+} MPCs were seen as early as E9.5 in both reporters, and the *Dll1*^{D1VmC}; *Hes1*-EGFP reporter revealed that these were adjacent to *Dll1*-expressing cells (Fig. 2e,j). The majority of cells in the E10.5 *Jag1*^{J1VmC}; *Hes1*-EGFP dorsal bud were Sox9^{+}EGFP^{+}mCherry^{+} MPCs, although EGFP^{+}mCherry^{-} cells were also seen (Fig. 2f) and again the EGFP^{+} cells were often Sox9^{Hi} and adjacent to Sox9^{Lo}mCherry^{+} cells in E10.5 *Dll1*^{D1VmC}; *Hes1*-EGFP buds (Fig. 2k). In E11.5 *Jag1*^{J1VmC}; *Hes1*-EGFP embryos, EGFP^{+}mCherry^{+} cells were seen mostly in the periphery while EGFP^{+}mCherry^{-} cells were abundant in the center (Fig. 2g). By E12.5, most of the center is occupied by emerging EGFP^{+}mCherry^{-} BPs while the periphery is mainly composed of nascent mCherry^{+} PACs interspersed with EGFP^{+}mCherry^{+} MPCs and rare EGFP^{+}mCherry^{-} cells (Fig. 2h). We frequently observed Sox9^{Hi}EGFP^{+}mCherry^{-} cells intercalated with Sox9$^{Lo/-}$EGFP^{-}mCherry^{+} cells in E11.5 and E12.5 *Dll1*^{D1VmC}; *Hes1*-EGFP pancreata (Fig. 2l,m), suggesting that high levels of Dll1 and Jag1 in PACs could mediate Notch *trans*-activation in neighboring Dll1$^{Lo/-}$Jag1$^{Lo/-}$ BPs. In E15.5 *Jag1*^{J1VmC}; *Hes1*-EGFP pancreata we found EGFP^{Hi} cells to be Sox9^{+}mCherry^{-} BPs located in the proximal "trunk" epithelium or occasionally in forming acini (Fig. 2i). In E15.5 *Dll1*^{D1VmC}; *Hes1*-EGFP pancreata, Sox9^{+}EGFP^{Hi} BPs were often in contact with Sox9$^{Lo/-}$mCherry^{+} cells and in the forming acini they were often found sandwiched between EGFP^{-}mCherry^{+} cells (Fig. 2n).

An important caveat to these analyses is the long half-life of the reporters. To overcome this, we used an anti-Hes1 antibody to map Notch activation in relation to ligand protein expression in E12.5 MPCs and emerging BPs and PACs, distinguished by their Ptf1a and Nkx6-1 expression status. We found most Hes1^{Hi} cells to be Nkx6-1^{Hi}Ptf1a$^{Lo/-}$Jag1$^{Lo/-}$ and most Hes1$^{Lo/-}$ cells to be Nkx6-1$^{Lo/-}$Ptf1a^{Hi}Jag1^{Hi} except for a few Hes1$^{Lo/-}$ cells that were Nkx6-1^{Hi}Ptf1a^{Hi}Jag1^{Hi} (Fig. 2o-q). In relation to Dll1, we found that Hes1^{Hi} cells typically were Nkx6-1^{Hi}Ptf1a$^{Lo/-}$Dll1$^{Lo/-}$ BPs, mostly emerging

centrally but in rare cases as single cells in the periphery located next to Hes1^{Lo}Nkx6-1$^{Lo/-}$Ptf1a^{Hi}Dll1^{Hi} cells (Fig. 2r-t).

As the ratio between ligands and receptors determines whether cells are prone to sending or receiving Notch signals we examined the distribution of Notch1 and Notch2, the two receptors known to be expressed in the pancreatic epithelium[32], at E12.5 using previously validated antisera[27]. While Notch1 was expressed in PACs and BPs (Fig. 2u-w), Notch2 was specifically enriched in BPs (Fig. 2x-z), as previously noted in E15.5 pancreas[27]. Thus, BPs (Jag1^{-}Dll1^{-}Notch1^{+}Notch2^{+}) may have receptors in stoichiometric surplus, favoring signal reception, while in PACs (Jag1^{+}Dll1$^{+/-}$Notch1^{+}Notch2^{-}) the ligands may be in surplus, favoring signal sending. Taken together, these data show that Notch receptor activation becomes suppressed in emerging Jag1^{+}Dll1$^{+/-}$ PACs, and support the notion that these, together with Ngn3^{+}Dll1^{Hi} endocrine precursors in the central trunk epithelium, are activating Notch receptors in nascent, Jag1$^{Lo/-}$Dll1$^{Lo/-}$ BPs.

Suppressing Notch before ~E13 shunts progenitors to a PAC fate. To define the temporal window through which Notch signaling controls segregation of MPCs into BP and PAC fates we administered tamoxifen (Tam) to pregnant dams carrying either *Hnf1b*-CreER^{T2}; *Rosa26*$^{LSL\text{-}dnMaml1\text{-}eGFP/+}$ (hereafter referred to as *R26*^{dnMaml1}) embryos or *Hnf1b*-CreER^{T2}; *Rosa26*$^{LSL\text{-}YFP/+}$ (hereafter referred to as *R26*^{YFP}) control embryos at different timepoints and harvested embryos for analysis at E15.5 (Fig. 3a). As expected from a previous *Hnf1b*-CreER^{T2} lineage-tracing analysis[6], IF examination of E11.5 Tam-treated *R26*^{YFP} pancreata for Sox9 and Ptf1a revealed that ~45% of the YFP^{+} cells expressed the BP marker Sox9, ~25% expressed Ptf1a, and ~30% expressed neither marker (Fig. 3b, n). In contrast, similarly treated *R26*^{dnMaml1} pancreata showed an ~11-fold reduction of GFP^{+} cells adopting a BP fate, while the fraction of GFP^{+} cells allocated to a PAC fate had increased almost 3-fold. The fraction of YFP^{+} cells expressing neither marker was unchanged (Fig. 3e, n).

In *R26*^{YFP} pancreata exposed to Tam at E12.5, about one third of the YFP^{+} cells were Sox9^{+} while ~20% expressed Ptf1a, and ~50% expressed neither marker (Fig. 3c,n). Tam injection at E13.5 revealed an even more pronounced distribution of control YFP^{+}

cells towards BP fate: ~50% of the YFP$^+$ cells were Sox9$^+$ and only ~8% of the YFP$^+$ cells were Ptf1a$^+$, while ~42% expressed neither marker (Fig. 3d,n). Thus, while some *Hnf1b*-expressing cells retain their multipotency at E13 and E14, they become progressively more biased towards the BP lineage, as also noted previously[6]. As observed for E11.5 Tam injections, significantly fewer EGFP$^+$ cells co-expressed Sox9 in E15.5 *R26*^{dnMaml1} pancreata injected with Tam at E12.5 or E13.5 compared to controls. However, in sharp contrast to E11.5 Tam-induced pancreata, the proportion of EGFP$^+$ cells expressing Ptf1a was unchanged following Tam treatment at E12.5 and E13.5. Instead, more EGFP$^+$ cells were Sox9$^-$Ptf1a$^-$, compared to YFP$^+$ cells in the controls (Fig. 3f,g,n). Together, these data show that suppression of Notch signal reception in MPCs and BPs before ~E13 shunts the cells to a PAC fate. However, if Notch signaling is blocked in BPs after ~E13, they adopt an alternative fate.

Suppressing Notch after ~E13 shunts progenitors to an endocrine fate. The location of the Sox9$^-$Ptf1a$^-$EGFP$^+$ cells seen in E15.5 *R26*^{dnMaml1} pancreata exposed to Tam at E12.5 or E13.5 suggests that these may represent cells of the endocrine lineage. However, it is less clear whether one would expect accumulation of endocrine precursors, endocrine cells or both. We therefore performed IF for EGFP/YFP, Sox9, Ngn3 and Chga. As expected, the fraction of labelled cells expressing Sox9 in E15.5 *R26*^{dnMaml1} pancreata was significantly lower than in controls after Tam injection at E11.5 and consistent with the increase of labelled Ptf1a$^+$ cells seen above in the same embryos, significantly more labelled cells triple-negative for Sox9, Ngn3 and Chga in dnMaml1 embryos, compared to controls (Fig. 3h,k,o). Examining endocrine lineage markers we found that the fraction of labelled cells expressing either Ngn3 or Chga, was not significantly different between dnMaml1 embryos and controls (Fig. 3h,k,o). However, fewer labelled cells co-expressed Ngn3 in dnMaml1 embryos than in controls (Fig. 3p).

Tam injections at E12.5 and E13.5 gave a different result. While the fraction of labelled cells expressing Sox9 was still reduced in dnMaml1 embryos compared to controls, the fraction of labelled cells expressing endocrine markers was now markedly increased compared to controls, while the fraction of labelled cells triple-negative for

Sox9, Ngn3 and Chga was unchanged between groups (Fig. 3i,j,l,m). Again, fewer labelled cells co-expressed Ngn3 in dnMaml1 embryos than in controls (Fig. 3p).

These findings were reproduced by lineage-tracing analyses in E15.5 *Sox9*-CreER^{T2}; *R26*^{dnMaml1} embryos compared to stage-matched *Sox9*-CreER^{T2}; *R26*^{YFP} embryos. A qualitative analysis of these revealed the same shift in the fate of the labelled cells when comparing Tam injections at E11.5 to E12.5 and E13.5 as described above for *Hnf1b*-CreER^{T2}-driven recombination (Supplementary Fig. 3). Taken together, these results show that the time window through which prevention of Notch activation can shunt cells to a PAC fate closes by ~E13 and confirms that prevention of Notch activation in BPs after ~E13 induces endocrine differentiation[26,27].

Jag1 is required to specify most BPs. To begin to understand the role of individual ligands in PD patterning we next generated conditional Jag1 and Dll1 mutants. Analysis of E12.5 *Dll1*; *Jag1*$^{\Delta Sox17\text{-}TamE6.5}$ single and double mutant embryos revealed an increase of Ptf1a^{+}Nkx6-1^{+} MPCs and a reduction of Ptf1a^{-}Nkx6-1^{+} BPs (Supplementary Fig. 4), suggesting that Jag1 and Dll1 are both involved in PD patterning. Due to the variable effect size and intrinsic mosaicism in such embryos we decided to employ *Foxa2*^{T2AiCre} (hereafter referred to as *Foxa2*^{iCre}) in further experiments to ensure efficient recombination prior to pancreas specification[19]. However, since *Foxa2* is linked to *Jag1* on mouse chromosome 2 at a distance of ~5.7 cM (Supplementary Fig. 5) we first introduced a *Jag1* null allele[38] on the same chromosome as the *Foxa2*^{iCre} allele via meiotic crossover. Animals carrying *Jag1*$^{-}$; *Foxa2*^{iCre} chromosomes were then backcrossed to homozygous *Foxa2*$^{iCre/iCre}$ animals to secure this chromosome from further crossover events. Timed matings of these mice with *Jag1*$^{fl/fl}$; *R26*$^{YFP/YFP}$ animals generated *Jag1*$^{\Delta Foxa2/-}$ embryos (referred to as *Jag1*$^{\Delta Foxa2}$) and *Jag1*$^{\Delta Foxa2/+}$ heterozygote littermate controls. Examination at E10.5 by whole-mount IF (WMIF) analysis revealed both the dorsal and ventral pancreata to be increased in size but with no evidence of excessive endocrine differentiation (Supplementary Fig. 5). At E12.5, the *Jag1*$^{\Delta Foxa2}$ mutant pancreas appeared grossly normal in size and morphology, yet IF analysis revealed that the number of Ptf1a^{+}Nkx6-1^{+} MPCs was significantly increased at the expense of Ptf1a^{-}Nkx6-1^{+} BPs compared to controls, and the staining intensity of Ptf1a also appeared consistently brighter (Fig. 4a-c). While Ptf1a is essentially confined to

the outermost epithelial cell layer in E12.5 controls (Fig. 4a, insert), Ptf1a expression was also seen in many proximal cells in *Jag1*$^{\Delta Foxa2}$ pancreata (Fig. 4b, insert). This shows that, similar to *Jag1*$^{\Delta Sox17\text{-}TamE6.5}$ embryos, the segregation of MPCs into PAC and BP domains is compromised in E12.5 *Jag1*$^{\Delta Foxa2}$ pancreata. IF analyses at later stages revealed that most Ptf1a^{+} cells co-expressed Nkx6-1 and Sox9 at E13.5, thus maintaining an MPC marker profile. Not until E14.5 did we observe a resolution into distinct Ptf1a^{+}Nkx6-1^{-} PACs and Ptf1a^{-}Nkx6-1^{+} BPs in the *Jag1*$^{\Delta Foxa2}$ pancreas. However, while BPs are normally extending all the way into the forming acini at this stage, the *Jag1*$^{\Delta Foxa2}$ pancreas was nearly devoid of such cells in the periphery, while the number of Ngn3^{+} endocrine precursors and insulin^{+} β-cells, appeared unaffected at these stages (Supplementary Fig. 6). Remarkably, one day later the *Jag1*$^{\Delta Foxa2}$ pancreas manifests a striking ~85-90% decrease in Nkx6-1^{+} and Sox9^{+} BPs relative to littermate controls with the few remaining BPs being confined to the center of the organ (Fig. 4d-i). The total number of cells is unchanged due to an equivalent increase of Ptf1a^{+} cells, suggesting that MPCs normally fated to become BPs switch to a PAC fate.

The combined activities of *Jag1* and *Dll1* specify the entire BP population. The residual ~10% proximal-most BPs observed in *Jag1*$^{\Delta Foxa2}$ pancreata may still require a Notch signal which Dll1 is likely to provide given its spatiotemporal expression pattern. To test this notion, we crossed *Jag1*$^{+/-}$; *Dll1*$^{fl/+}$; *Foxa2*$^{T2AiCre/T2AiCre}$ with *Jag1*$^{fl/fl}$; *Dll1*$^{fl/fl}$; *R26*$^{YFP/YFP}$ mice to generate compound *Jag1*; *Dll1*$^{\Delta Foxa2}$ mutants. For comparison, we used stage-matched single *Dll1*$^{\Delta Foxa2}$ and *Jag1*$^{\Delta Foxa2}$ mutants as well as control mice without ligand deletions (*Foxa2*^{T2AiCre}*; R26*^{YFP}). Analysis of all four genotypes at E15.5 revealed no change in the numbers of Ptf1a^{+}Nkx6-1^{-} PACs or Ptf1a^{-}Nkx6-1^{+} BPs between single *Dll1*$^{\Delta Foxa2}$ mutant and control pancreata. As expected, Ptf1a^{-}Nkx6-1^{+} BPs were severely depleted in *Jag1*$^{\Delta Foxa2}$ mutants and we noted a concomitant expansion in Ptf1a^{+}Nkx6-1^{-} PAC, while compound *Jag1*; *Dll1*$^{\Delta Foxa2}$ mutants showed an even more profound loss of Ptf1a^{-}Nkx6-1^{+} BPs and increase in Ptf1a^{+}Nkx6.1^{-} PACs over either single mutant (Fig. 5a-e). The confinement of the remaining Nkx6-1^{+} BPs to the central core in *Jag1*$^{\Delta Foxa2}$ mutants, was confirmed and extended to *Jag1*; *Dll1*$^{\Delta Foxa2}$ mutants by quantifying the fraction of Nkx6-1^{+} and Ptf1a^{+} cells in the *z*-dimension (Fig. 5f). Since Nkx6-1 is expressed in both BPs and β-cells we next analyzed Sox9^{+} and

insulin$^+$ cell numbers to distinguish between the two. While Sox9$^+$ BPs were unchanged in E15.5 *Dll1*$^{\Delta Foxa2}$ mutants compared to wild types, they were severely reduced in *Jag1*$^{\Delta Foxa2}$ mutants and even more so in compound *Jag1*; *Dll1*$^{\Delta Foxa2}$ mutants (Fig. 5g-k). As expected from the loss of BPs, assessment of endocrine differentiation by IF analysis of Ngn3 and insulin revealed a loss of BP progeny by E15.5. An ~50% decrease in the number of insulin$^+$ β-cells was seen in both *Dll1*$^{\Delta Foxa2}$ and *Jag1*$^{\Delta Foxa2}$ compared to littermate control pancreata, while compound *Jag1*; *Dll1*$^{\Delta Foxa2}$ mutants exhibited a more profound loss than either single mutant alone (Fig. 5g-l). Together, these data show that the combined activities of Jag1 and Dll1 are crucial for proper PD patterning of the mouse pancreas epithelium.

Impeding ligand trans-activation in late development only affects CACs. The strong phenotype we observe in *Jag1*; *Dll1*$^{\Delta Foxa2}$ mutant embryos contrasts with the rather modest phenotype seen in *Jag1*; *Dll1*$^{\Delta Ptf1a}$ mutant embryos, which only lack CACs[34]. This suggests that the timing of Cre-mediated recombination, which is mosaic and occurs considerably later with *Ptf1a*^{Cre} compared with *Foxa2*^{iCre} [44,48], is critical for deciding the outcome. Considering that Mib1 is required for all Notch ligand trans-activation[39-41] and that its elimination in *Mib1*$^{\Delta Foxa2}$ pancreata phenocopies the cell fate changes in *Jag1*; *Dll1*$^{\Delta Foxa2}$ embryos seen here[19], we therefore asked whether *Mib1*$^{\Delta Ptf1a}$ pancreata would phenocopy *Jag1*; *Dll1*$^{\Delta Ptf1a}$ pancreata. *Mib1*-depleted cells and their progeny were identified by *R26*^{YFP} recombination. Examination of *Mib1*$^{\Delta Ptf1a}$ pancreata prior to E13.5 failed to reveal any obvious defects. In contrast, analysis at E15.5 revealed the ductal tree to be truncated distally. The distal-most, Sox9$^+$ prospective CACs which normally protrude into the nascent Ptf1a$^+$ acini are specifically depleted in *Mib1*$^{\Delta Ptf1a}$ embryos (Supplementary Fig. 7). Notably, this phenotype closely resembles the reported loss of CACs following *Ptf1a*^{Cre}-driven compound deletion of *Dll1* and *Jag1*[34]. Taken together, these results suggest that the trans-activation of Notch receptors by Jag1 and Dll1 expressed on PACs and emerging acinar cells is required to specify and/or maintain adjacent terminal BPs/CAC precursors.

Early *Jag1*$^{\Delta Foxa2}$ mutants have normal plexus formation and organ architecture. We next analyzed how the BP-to-PAC fate switch affects ductal morphogenesis and overall

organ development. In spite of the delayed PD patterning, we found that formation of the epithelial plexus occurred normally in E12.5 *Jag1*$^{\Delta Foxa2}$ mutants and overall organ size and morphology was comparable between *Jag1*$^{\Delta Foxa2}$ mutants and control littermates (Fig. 6a-d). Remarkably, even at E15.5 the overall organ architecture of *Jag1*$^{\Delta Foxa2}$ mutants is essentially unaffected. The *Jag1*$^{\Delta Foxa2}$ dorsal pancreas had a well-formed, anvil-shaped head and the body gradually tapered into the narrow connection with a normal-sized ventral pancreas located in the duodenal loop (Fig. 6e,f). In contrast, the *Dll1*$^{\Delta Foxa2}$ dorsal pancreas was hypoplastic with the head being malformed and the body of the pancreas being greatly shortened (Fig. 6g,h). However, closer inspection of *Jag1*$^{\Delta Foxa2}$ embryos revealed that although the ductal plexus appeared to have remodeled into a hierarchical tree-like structure, the smooth walls of the intercalated ducts seen in controls and *Dll1*$^{\Delta Foxa2}$ mutants, showed a more serrated appearance in *Jag1*$^{\Delta Foxa2}$ mutants (Fig. 6i-p). Nevertheless, acinar structure appears normal with apical localization of Muc1, ZO-1 and PKCζ, indicating that acinar cytoarchitecture is maintained in the E15.5 *Jag1*$^{\Delta Foxa2}$ pancreas (Supplementary Fig. 8). In the domain usually occupied by Sox9^{+} prospective ducts, we were able to identify elongated tubular structures expressing Ptf1a instead of Sox9 (Fig. 6q,r). Similar to normal PACs these mis-specified PACs also expressed Bhlha15/Mist1 (Fig. 6s,t). Taken together, these findings suggest that the overall organ architecture and remodeling of the ductal plexus is regulated independently from the differentiation programs that allocate MPCs to endocrine, duct and acinar lineages. In contrast, finer morphological features of the ductal tree are clearly perturbed by the BP-to-PAC fate switch.

Late *Jag1*$^{\Delta Foxa2}$ embryos show signs of acute pancreatitis and ADM. E18.5 *Jag1*$^{\Delta Foxa2}$ pancreata remained equivalent to controls in size and overall organ morphology. The dorsal and ventral pancreas appeared fused normally, the gastric lobe was present, and the normal "anvil" shape of the dorsal pancreas[42] was evident (Fig. 7a,b). However, closer inspection revealed that the larger ducts were not formed properly. The main duct was disrupted, and interlobular as well as larger intralobular ducts were largely absent (Fig. 7c-f and Supplementary Fig. 9). Again, many of the terminal ducts appeared serrated, occasionally connected by ducts of relatively normal morphology despite being composed of Ptf1a^{+}Mist1^{+} cells (Fig. 7c-f). As expected, we saw a

prominent loss of endocrine cells in E18.5 *Jag1*$^{\Delta Foxa2}$ pancreata, with scattered α-cells and a central cluster of β-cells. The late-arising, somatostatin^{+} δ-cells were nearly absent, even in the central cluster and examination of Muc1 and Krt19 expression and DBA lectin binding revealed an obvious paucity of the ductal tree and throughout the epithelium we observed numerous "ring-like" structures with perturbed apicobasal polarity and co-expression of amylase, Cpa1 and Krt19 (Fig. 7g-k, Supplementary Fig. 8, and Supplementary Fig. 9), reminiscent of the acinar-to-ductal metaplasia (ADM) associated with Cerulein-induced acute pancreatitis[43].

Increased Hes1 expression in *Jag1*$^{\Delta Foxa2}$ mutant MPCs. To begin to understand the mechanism causing progenitors to almost exclusively adopt a PAC fate we assessed how loss of Jag1 impacts Notch activity in *Jag1*$^{\Delta Foxa2}$ pancreata by IF analysis of Hes1 expression. We found that Hes1 expression, and by inference active Notch signaling, was upregulated in the E12.5 *Jag1*$^{\Delta Foxa2}$ pancreas compared to control littermates (Fig. 8a,b). This was especially notable in the distal-most cells, in which average Hes1 levels were increased ~2-fold (Fig. 8c). This finding suggests that Jag1 is required cell-autonomously to inhibit Notch activation in emerging PACs, which is somewhat surprising considering that *Mib1*$^{\Delta Foxa2}$, which lose Hes1 expression, and *Hes1*$^{\Delta Foxa2}$ pancreata show the same BP-to-PAC fate switch[19]. However, given that Notch signaling maintains the MPC fate[22], it does explain the persistence of the MPC marker profile in most epithelial cells in E12.5 *Jag1*$^{\Delta Foxa2}$ pancreata.

We therefore analyzed Hes1 expression in *Jag1*$^{\Delta Foxa2}$ pancreata at E14.5, and saw fewer Hes1^{Hi} cells in the epithelium of *Jag1*$^{\Delta Foxa2}$ pancreas compared to control (Fig. 8d, e). In contrast, Dll1 expression appeared similar in controls and mutants at these stages. Together, these findings suggest that Notch signaling is maintained in most of the epithelial cells in *Jag1*$^{\Delta Foxa2}$ pancreata, most likely by Dll1, but becomes suppressed around E14.5, which favors the PAC fate.

Discussion

In this study we show that the Notch ligand Jag1 is crucial for PD patterning of the developing mouse pancreas. The requirement for Notch signaling in MPC proliferation

and choice of BP versus PAC fate has been comprehensively documented by previous work[15-18,20-22,27,36,44,45]. Here we extend these studies by defining the temporal window of Notch dependent MPC segregation and by uncovering Jag1 as a crucial ligand for regulating MPC proliferation as well as coordinating the timely exit from the multipotent stage and proper PD patterning. We first found Jag1 uniformly expressed in ~E10.5 MPCs with a subset of MPCs showing heterogeneous co-expression of Dll1. Recently, initial experiments in our labs have shown that Dll1 (and Hes1) expression exhibits ultradian oscillations in the developing pancreas (*data not shown*) making this heterogeneity a likely result of catching oscillating cells in their peak phase[46]. We have previously shown that Dll1-deficient E10.5 pancreata are hypoplastic due to reduced proliferation[19,22,28] and initial experiments have shown that E10.5 *Dll1* Type 1 and Type 2 mutants, in which both Dll1 and Hes1 oscillations are dampened[47], also present with pancreatic hypoplasia albeit less severe than in $Dll1^{-/-}$ and $Dll1^{\Delta Foxa2}$ mutants (*data not shown*). Here we found the opposite phenotype in E10.5 Jag1-deficient pancreata, which are hyperplastic, suggesting that Jag1 antagonizes Dll1 function at this stage, possibly by a *cis*-inhibitory interaction that sequesters a fraction of the available Notch receptors. We propose that Jag1 provides a dampening tone on Notch activation mediated by oscillating Dll1 expression. Ultradian Dll1 oscillations then enables a temporal symmetry where MPCs alternate between sending and receiving input via Notch that ultimately couples to the mitotic machinery (Fig. 9a).

In pancreata undergoing PD patterning, we found that emerging PACs ($Ptf1a^{+}$) expressed high levels of ligands and little to no Hes1, indicating a state of low Notch activity. Conversely, adjacent MPCs ($Ptf1a^{+}Nkx6\text{-}1^{+}$) or BPs ($Nkx6\text{-}1^{+}$) were generally expressing no or low levels of ligand and high levels of Hes1, indicating Notch activation. This suggests that mutually inactivating *cis*-interactions between ligands and receptors[48] are crucial for exiting the multipotent stage and for the cells to adopt either a PAC or BP fate. Such a notion is supported by the downregulation of Hes1 and absence of Notch2 expression in PACs and thus overall lower levels of Notch receptor expression than seen in emerging $Notch1^{+}Notch2^{+}$ BPs. Conversely, Notch1/2 co-expression, and the absence of Jag1 expression in nascent BPs, would render these more sensitive to signal reception and less prone to signal emission due to *cis* interactions (Fig. 9b).

To test these ideas and to investigate the role of individual ligands in PD patterning we performed single and double Dll1/Jag1 loss-of-function experiments. Our marker analyses showed that most epithelial cells in the E12.5 *Jag1*$^{\Delta Foxa2}$ embryos maintained a Ptf1a^{+}Nkx6-1^{+}Sox9^{+} marker profile suggestion that they failed to exit the MPC stage. This correlated with increased Hes1 expression, suggesting that Notch activity is increased and that Jag1 normally acts cell-autonomously to inhibit Notch activation in emerging PACs. We suggest that upregulation of Jag1 *cis*-inhibits Notch receptors and thus acts as a symmetry breaker that terminates oscillatory Hes1 expression in nascent PACs. Loss of Notch activity may additionally downregulate Nkx6-1[18] and/or liberate Rbpj from N1ICD, which would then be free to complex with Ptf1a[49]. Both of these mechanisms would favor a PAC fate[15,49]. Concurrently, free ligand molecules would be able to convey *trans*-activation of receptors in neighboring cells if these are in a responsive, ligand^{Lo}/receptor^{Hi} state, and instruct these to adopt a BP fate (Fig. 9b).

In spite of increased Notch activity at early stages, *Jag1*$^{\Delta Foxa2}$ MPCs eventually adopt a PAC fate, which depends on the cells attaining a state of low Notch activation[15,18,19]. Indeed, we find that coincident with adoption of a PAC fate around E14.5, the number of Hes1^{Hi} cells is reduced in *Jag1*$^{\Delta Foxa2}$ mutant epithelium, indicating that most of the cells have acquired a state of low Notch activation at this stage. The decline in *Notch1* mRNA expression seen at this stage[32] is also indicative of reduced Notch activation[50]. However, it remains to be determined what triggers a reduction in Notch activation, but it is noteworthy that the timing coincides with the onset of *Lfng* (*Lunatic fringe*) expression at E14.5 in PACs[51]. Lunatic fringe has been shown to inhibit Notch activity in presomitic mesoderm[52] and could potentially strengthen *cis*-inhibitory activity of Dll1[53] in E14.5 *Jag1*$^{\Delta Foxa2}$ progenitors. This would attenuate expression of the BP-promoting Notch target genes Nkx6-1[18] and Sox9[27] in Dll1^{Hi} cells allowing these to exit from the MPC state and ultimately adopt a PAC fate (Fig. 9c). Testing this hypothesis and identifying the precise role of different Notch receptors awaits future experiments.

The strong effect on PD patterning we observe is surprising since previous analyses of pancreas-specific Jag1 or Jag1/Dll1 deletions did not uncover a prominent expansion of the PAC domain at the expense of BPs[33-35] . We suspect that this can be attributed to the different timing of efficient, non-mosaic recombination between different Cre

lines. Conditional Jag1 deletion with *Pdx1*-Cre or *Foxa3*^{Cre} driver lines occurs much later than with our targeted *Foxa2*^{Cre} driver, which recombined with >99% efficacy prior to pancreas specification[19]. More recently, compound *Dll1*; *Jag1*$^{\Delta Ptf1a}$ mutants were found to have a loss of CACs, the terminal-most cell type in the ductal tree, while single mutant littermates did not show any phenotype. As our *Mib1*$^{\Delta Ptf1a}$ mutants phenocopy the loss of CACs reported in *Dll1*; *Jag1*$^{\Delta Ptf1a}$ mutants, this suggests that the *Ptf1a*^{Cre}-driver only becomes non-mosaic in PACs and their progeny and that CACs are specified by PACs late in pancreatic development.

In spite of the prolonged MPC state, the ductal plexus forms normally. However, at later stages the consequence of the BP-to-PAC switch becomes evident as normal remodeling of the ductal plexus into a well-structured ductal tree is disrupted. The tubular network making up the intercalated ducts seems to form but the normal smooth morphology of the ductal lumen is perturbed by E15.5. We also noted a complete absence of larger intralobular ducts and interlobular ducts at E18.5 and ductal structures in the area of the main duct appear interrupted as also previously noted in *Jag1*$^{\Delta Pdx1}$ animals[33]. These perturbations are not surprising given that acinar cells are not designed to form cuboidal or columnar epithelia, but rather to adopt a pyramidal shape fitting for cells forming an acinus. However, in spite of these disturbances the overall organ architecture is surprisingly well preserved. We conclude that the regulatory principles governing the shape of the pancreas are highly resilient to cell fate changes, at least as long as these occur in the internal part of the organ.

Methods

Animals. Published mouse strains were genotyped according to the original work: *R26*$^{LSL\text{-}dnMaml1\text{-}EGFP}$ [19], *Gt(ROSA)26Sortm1(EYFP)Cos* (*R26*$^{LSL\text{-}YFP}$ reporter[54]), *Gt(ROSA)26Sortm3*(CAG-EYFP)Hze (*R26*$^{LSL\text{-}Ai3}$ reporter[55]), *Mib1*^{tm2Kong} (floxed *Mib1*[41]), *Dll1*^{tm1Gos} (*Dll1*^{LacZ} null allele[56]), *Dll1*$^{tm1.1Hri}$ (floxed *Dll1*[19]), *Jag1*^{tm1Grid} (*Jag1* null allele[38]), *Jag1*^{tm2Grid} (floxed *Jag1*[57]), Tg(Hes1-EGFP)^{1Hri} (BAC transgenic *Hes1-EGFP* reporter[24]), *Hes1*^{tm1Fgu} (*Hes1* null allele[58]), *Foxa2*^{T2AiCre} (Cre add-on allele[19]), *Hnf1b*-CreER^{T2} [6], *Sox9*-CreER^{T2} [4], *Sox17*^{T2AiCre} [59], *Ptf1a*^{Cre} [60] and *Notch1*$^{tm4(cre)Rko}$ (N1IP::Cre^{HI} [37]). Additional

genotyping primers are given in Supplementary Table 1. Homozygous *Dll1*^{D1VmC} and *Jag1*^{J1VmC} mice are viable and fertile, but were maintained and analyzed as heterozygotes due to *Dll1*^{D1VmC} being a weak hypomorph evident by short, kinky tails in homozygote animals. The *Sox17*^{CreERT2} line, which was generated by cassette exchange in the *Sox17*^{LCA} allele[61], was a kind gift by Anne Grapin-Botton. Generation of Jag1 C-terminal Venus-T2A-mCherry fusion reporter knock-in construct was conducted using a BAC clone (RP23-173O12) from the BACPAC Resources Center at Children's Hospital Oakland Research Institute. An frt-PGK-EM7-Neo-frt cassette was inserted downstream of a Venus-T2A-mCherry reporter in pBluescript II SK+, flanked by 300-500-bp homology arms from the *Jag1* gene with the *Jag1* stop codon removed. BAC targeting cassettes were excised and electroporated into competent SW105 cells containing the BAC clone of interest. Correctly targeted BAC clones were identified by a panel of PCR primers and restriction digestions. The knock-in cassette fragment was retrieved and cloned into pMCS-DTA (a kind gift from Dr. Kosuke Yusa, Osaka University, Japan). The 5'- and 3'-homology arms in the retrieval vector were designed such that between 2.5- and 7.5-kb DNA segments, flanking the Venus-T2A-mCherry reporter-frt-PGK-EM7-Neo-frt cassette in the BAC clone, were subcloned into pMCS-DTA. The shorter homology arm was used to design PCR-based screening for targeted ES cells (TT2). Chimeric mice were produced from successfully targeted ES cell clones by aggregation with ICR embryos. Germ line transmission of the targeted allele was assessed by PCR of tail DNA. pCAG-FLPe mice[62] were used to remove the frt-PGK-EM7-Neo-frt cassette. The Dll1-Venus-T2A-mCherry knock-in mice were generated by a similar strategy using a *Dll1* containing BAC clone (RP23-306J23).

Noon on the day of vaginal plug appearance was considered E0.5. Tamoxifen (Sigma) was dissolved at 10 mg/ml in corn oil (Sigma) and a single dose of 75 μg/g (for *Hnf1b*- and *Sox9*-CreER^{T2}-mediated *R26*$^{YFP/dnMaml1\text{-}eGFP}$ induction) or 40 μg/g (for *Sox17*^{CreERT2}-mediated ligand deletion) body-weight administered by intraperitoneal injection at noon ± 1 hour. *Jag1*$^{\Delta Foxa2}$ and *Dll1*; *Jag1*$^{\Delta Foxa2}$: We first introduced a *Jag1* null allele[38] on the chromosome carrying the *Foxa2*^{iCre} allele via meiotic crossover. Animals carrying *Jag1*$^{-}$; *Foxa2*^{iCre} chromosomes were then backcrossed to homozygous *Foxa2*$^{iCre/iCre}$ animals to secure this chromosome from further crossover events. *Jag1*$^{+/-}$; *Foxa2*$^{iCre/iCre}$ animals were next crossed with *Jag1*$^{fl/fl}$*R26*$^{YFP/YFP}$ animals to generate

Jag1$^{\Delta Foxa2}$ embryos and to *Dll1*$^{fl/+}$; *Foxa2*$^{T2AiCre/T2AiCre}$ animals to generate *Jag1*$^{+/-}$; *Dll1*$^{fl/+}$; *Foxa2*$^{T2AiCre/T2AiCre}$ mice. The latter was then crossed with *Jag1*$^{fl/fl}$; *Dll1*$^{fl/fl}$; *R26*$^{YFP/YFP}$ animals to generate *Jag1*; *Dll1*$^{\Delta Foxa2}$ embryos. *Dll1*$^{\Delta Foxa2}$ embryos and *R26*^{YFP} controls were made as previously described[19]. All animal experiments described herein were conducted in accordance with local legislation and authorized by the local regulatory authorities.

Immunostaining. All primary antibodies are listed with dilution in Supplementary Table 2. Dissected whole embryos (E10.5-E12.5) and foregut preparations (E13.5-E18.5) were fixed in 4% paraformaldehyde in PBS, embedded in Tissue-Tek O.C.T. (Sakura Finetek) and cryosectioned at 10 μm. For immunofluorescence analysis, antigen retrieval was conducted in pH6.0 citrate buffer, followed by permeabilization in 0.15% Triton X-100 in PBS. After blocking in 1% normal donkey serum in PBS with 0.1% Tween-20, sections were incubated overnight at 4°C with primary antibodies diluted in the same buffer. Primary antibodies were detected with anti-rabbit, guinea pig, mouse, rat, goat, sheep or chicken donkey-raised secondary antibodies conjugated to either Cy5 (1:500), Cy3 (1:1,000), Alexa Fluor 488 (1:1,000) or DyLight 405 (1:200) (all Jackson ImmunoResearch Laboratories). Slides were mounted in Vectashield (Vector Laboratories) with or without DAPI for counterstaining nuclei. Whole-mount IF of E10.5 whole embryos and E12.5, E15.5 and E18.5 foregut preparations was performed as previously described[63]. Specimens were cleared with BABB (benzyl alcohol:benzyl benzoate 1:2) then scanned confocally for *z*-stack image acquisition. Images were captured on a Leica SP8 or Zeiss LSM780 confocal microscope and figures prepared using Adobe Photoshop/Illustrator CS6 (Adobe Systems, San Jose, CA, USA).

Antibody validation. Antisera against Dll1, Jag1, and Hes1 were validated by IF analysis of E10.5 neural tube from embryos that were either wildtype or null for the relevant gene (Supplementary Fig. 10). Two characteristic stripes of Jag1 was detected in the neural tube[64] and uniform but weak Jag1 was detected in the E10.5 pancreas by both anti-Jag1 antisera in wild type tissue, but not in equivalent *Jag1*-null[38] tissue. The anti-Dll1 antibody detected Dll1 in the expected reciprocal pattern (compared to

Jag1[38]) in the neural tube and scattered cells in the pancreas of wild type embryos, but not *Dll1*$^{-/-}$ embryos[56]. The rabbit anti-Hes1 monoclonal detected Hes1 in the expected patterns in both wild type tissues (i.e. prominently in floor plate and dorsal neural tube as well as pancreatic epithelium and weakly in the surrounding mesenchyme), but not in *Hes1*$^{-/-}$ tissues.

Cell quantification. ~400 cells YFP^{+} lineage-traced cells were counted on 9-11 evenly spaced optical sections from each of three E12.5 N1IP::Cre^{HI}; *Rosa26*$^{LSL\text{-}Ai3}$ embryos and scored for co-expression of Sox9 and Ptf1a. YFP^{+} and GFP^{+} lineage-traced cells from *Hnf1b*-CreER^{T2}; *R26*^{YFP} and *R26*$^{dnMaml1\text{-}GFP}$ embryos, respectively, were counted on every fifth section throughout the pancreas, for a total of >200 cells/embryo, for each marker combination. Ptf1a^{+}Nkx6.1^{-}, Ptf1a^{-}Nkx6.1^{+} and Ptf1a^{+}Nkx6.1^{+} cells were manually scored on every fifth section throughout E12.5 dorsal pancreas from controls (*R26*$^{Yfp/+}$; *Sox17*$^{CreERT/+}$), *Dll1*$^{\Delta Sox17Tam}$, *Jag1*$^{\Delta Sox17Tam}$, *Dll1/Jag1*$^{\Delta Sox17Tam}$ using Imaris™ (Bitplane). E12.5 *Jag1*$^{\Delta Foxa2}$ embryos were quantified the same way but with their own controls (see below). For quantification of E12.5 *Jag1*$^{\Delta Foxa2}$ Hes1 IF signal intensity in distal-most Ptf1a^{+} cells, corrected total cell fluorescence (CTCF) was determined using FIJI[65,66]. Numbers of Ptf1a^{+}Nkx6.1^{-}, Ptf1a^{-}Nkx6.1^{+} and Ptf1a^{+}Nkx6.1^{+} cells as well as Sox9^{+} and insulin^{+} cells were manually scored from every tenth section of dorsal pancreata from E15.5 controls (*R26*$^{Yfp/+}$; *Foxa2*$^{iCre/+}$; *Dll1*$^{+/+}$; *Jag1*$^{+/+}$), *Jag1*$^{\Delta Foxa2}$, *Dll1*$^{\Delta Foxa2}$ and *Jag1/Dll1*$^{\Delta Foxa2}$ embryos and expressed relative to the area (in mm^2) of the YFP^{+} dorsal pancreatic epithelium using FIJI.

Statistical analyses. The data were analyzed using Student's *t* test using 2-tailed analysis (GraphPad), except where otherwise noted. All tests were unpaired except for Hes1 IF CTCF quantification, where a paired *t* test was used to compare *Jag1*$^{\Delta Foxa2}$ with *control* values collected from three separate pairs of mutants/littermate controls in three independent analyses. Data are presented as mean ± S.D. and the sample number (indicated in figure legends) was a minimum of three embryos per genotype, except for *Jag1*; *Dll1*$^{\Delta Foxa2}$ for which we so far have only been able to collect two embryos.

Acknowledgements. We thank Ole D. Madsen and Jane E. Johnson for antibodies, Young-Yun Kong, Jorge Ferrer, Heiko Lickert, Chris V.E. Wright, Anne Grapin-Botton and Mark A. Magnuson for mouse lines, and Thi Nguyen for technical assistance. P.S. received grants from the Novo Nordisk Foundation (NNF16076 and NNF10717). The Novo Nordisk Foundation Center for Stem Cell Biology is supported by a Novo Nordisk Foundation grant number NNF17CC0027852.

Author Contributions. P.A.S. and C.A.C designed, carried out experiments and wrote the manuscript. M.C.J. performed all staining, imaging and quantitative analysis of whole-mount specimens. K.H.L. contributed to phenotype analysis. I.I. and R.Ka. generated the *Jag1*^{J1VmC} and *Dll1*^{D1VmC} mouse lines. T.N. and R.Ko. generated the N1IP::Cre^{HI}; *Rosa26*$^{LSL\text{-}Ai3}$ embryos. P.S. conceived the study, designed and interpreted experiments and wrote the manuscript. All authors revised and approved the manuscript.

Competing Interests. The authors declare no competing or financial interests.

References

1 Shih, H. P., Wang, A. & Sander, M. Pancreas organogenesis: from lineage determination to morphogenesis. *Annu Rev Cell Dev Biol* **29**, 81-105, doi:10.1146/annurev-cellbio-101512-122405 (2013).

2 Wessells, N. K. & Cohen, J. H. Early Pancreas Organogenesis: Morphogenesis, Tissue Interactions, and Mass Effects. *Dev Biol* **15**, 237-270 (1967).

3 Gu, G., Dubauskaite, J. & Melton, D. A. Direct evidence for the pancreatic lineage: NGN3+ cells are islet progenitors and are distinct from duct progenitors. *Development* **129**, 2447-2457 (2002).

4 Kopp, J. L. *et al.* Sox9+ ductal cells are multipotent progenitors throughout development but do not produce new endocrine cells in the normal or injured adult pancreas. *Development* **138**, 653-665, doi:10.1242/dev.056499 (2011).

5 Pan, F. C. *et al.* Spatiotemporal patterns of multipotentiality in Ptf1a-expressing cells during pancreas organogenesis and injury-induced facultative restoration. *Development* **140**, 751-764, doi:10.1242/dev.090159 (2013).

6 Solar, M. *et al.* Pancreatic exocrine duct cells give rise to insulin-producing beta cells during embryogenesis but not after birth. *Dev Cell* **17**, 849-860, doi:10.1016/j.devcel.2009.11.003 (2009).

7 Zhou, Q. *et al.* A multipotent progenitor domain guides pancreatic organogenesis. *Dev Cell* **13**, 103-114, doi:10.1016/j.devcel.2007.06.001 (2007).

8 Larsen, H. L. *et al.* Stochastic priming and spatial cues orchestrate heterogeneous clonal contribution to mouse pancreas organogenesis. *Nat Commun* **8**, 605, doi:10.1038/s41467-017-00258-4 (2017).

9 Ahlgren, U., Pfaff, S. L., Jessell, T. M., Edlund, T. & Edlund, H. Independent requirement for ISL1 in formation of pancreatic mesenchyme and islet cells. *Nature* **385**, 257-260, doi:10.1038/385257a0 (1997).

10 Pictet, R. L., Clark, W. R., Williams, R. H. & Rutter, W. J. An ultrastructural analysis of the developing embryonic pancreas. *Dev Biol* **29**, 436-467 (1972).

11 Spooner, B. S., Walther, B. T. & Rutter, W. J. The development of the dorsal and ventral mammalian pancreas in vivo and in vitro. *J Cell Biol* **47**, 235-246 (1970).

12 Villasenor, A., Chong, D. C. & Cleaver, O. Biphasic Ngn3 expression in the developing pancreas. *Dev Dyn* **237**, 3270-3279, doi:10.1002/dvdy.21740 (2008).

13 Gradwohl, G., Dierich, A., LeMeur, M. & Guillemot, F. neurogenin3 is required for the development of the four endocrine cell lineages of the pancreas. *Proc Natl Acad Sci U S A* **97**, 1607-1611 (2000).

14 Hald, J. *et al.* Generation and characterization of Ptf1a antiserum and localization of Ptf1a in relation to Nkx6.1 and Pdx1 during the earliest stages of mouse pancreas development. *J Histochem Cytochem* **56**, 587-595, doi:10.1369/jhc.2008.950675 (2008).

15 Schaffer, A. E., Freude, K. K., Nelson, S. B. & Sander, M. Nkx6 transcription factors and Ptf1a function as antagonistic lineage determinants in

multipotent pancreatic progenitors. *Dev Cell* **18**, 1022-1029, doi:10.1016/j.devcel.2010.05.015 (2010).

16 Hald, J. *et al.* Activated Notch1 prevents differentiation of pancreatic acinar cells and attenuate endocrine development. *Dev Biol* **260**, 426-437 (2003).

17 Murtaugh, L. C., Stanger, B. Z., Kwan, K. M. & Melton, D. A. Notch signaling controls multiple steps of pancreatic differentiation. *Proc Natl Acad Sci U S A* **100**, 14920-14925, doi:10.1073/pnas.2436557100 (2003).

18 Afelik, S. *et al.* Notch-mediated patterning and cell fate allocation of pancreatic progenitor cells. *Development* **139**, 1744-1753, doi:10.1242/dev.075804 (2012).

19 Horn, S. *et al.* Mind bomb 1 is required for pancreatic beta-cell formation. *Proc Natl Acad Sci U S A* **109**, 7356-7361, doi:10.1073/pnas.1203605109 (2012).

20 Apelqvist, A. *et al.* Notch signalling controls pancreatic cell differentiation. *Nature* **400**, 877-881 (1999).

21 Jensen, J. *et al.* Control of endodermal endocrine development by Hes-1. *Nat Genet* **24**, 36-44 (2000).

22 Ahnfelt-Rønne, J. *et al.* Ptf1a-mediated control of Dll1 reveals an alternative to the lateral inhibition mechanism. *Development* **139**, 33-45 (2012).

23 Bankaitis, E. D., Bechard, M. E. & Wright, C. V. Feedback control of growth, differentiation, and morphogenesis of pancreatic endocrine progenitors in an epithelial plexus niche. *Genes Dev* **29**, 2203-2216, doi:10.1101/gad.267914.115 (2015).

24 Klinck, R. *et al.* A BAC transgenic Hes1-EGFP reporter reveals novel expression domains in mouse embryos. *Gene expression patterns : GEP* **11**, 415-426, doi:10.1016/j.gep.2011.06.004 (2011).

25 Kopinke, D. *et al.* Lineage tracing reveals the dynamic contribution of Hes1+ cells to the developing and adult pancreas. *Development* **138**, 431-441, doi:10.1242/dev.053843 (2011).

26 Magenheim, J. *et al.* Ngn3(+) endocrine progenitor cells control the fate and morphogenesis of pancreatic ductal epithelium. *Dev Biol* **359**, 26-36, doi:10.1016/j.ydbio.2011.08.006 (2011).

27 Shih, H. P. *et al.* A Notch-dependent molecular circuitry initiates pancreatic endocrine and ductal cell differentiation. *Development* **139**, 2488-2499, doi:10.1242/dev.078634 (2012).

28 Jorgensen, M. C. *et al.* Neurog3-dependent pancreas dysgenesis causes ectopic pancreas in Hes1 mutants. *Development*, doi:10.1242/dev.163568 (2018).

29 Lorent, K. *et al.* Inhibition of Jagged-mediated Notch signaling disrupts zebrafish biliary development and generates multi-organ defects compatible with an Alagille syndrome phenocopy. *Development* **131**, 5753-5766, doi:10.1242/dev.01411 (2004).

30 Yee, N. S., Lorent, K. & Pack, M. Exocrine pancreas development in zebrafish. *Dev Biol* **284**, 84-101, doi:10.1016/j.ydbio.2005.04.035 (2005).

31 Zhang, D. *et al.* Endoderm Jagged induces liver and pancreas duct lineage in zebrafish. *Nat Commun* **8**, 769, doi:10.1038/s41467-017-00666-6 (2017).

32 Lammert, E., Brown, J. & Melton, D. A. Notch gene expression during pancreatic organogenesis. *Mechanisms of development* **94**, 199-203 (2000).

33 Golson, M. L., Loomes, K. M., Oakey, R. & Kaestner, K. H. Ductal malformation and pancreatitis in mice caused by conditional Jag1 deletion. *Gastroenterology* **136**, 1761-1771 e1761, doi:10.1053/j.gastro.2009.01.040 (2009).

34 Nakano, Y. *et al.* Disappearance of centroacinar cells in the Notch ligand-deficient pancreas. *Genes Cells* **20**, 500-511, doi:10.1111/gtc.12243 (2015).

35 Golson, M. L. *et al.* Jagged1 is a competitive inhibitor of Notch signaling in the embryonic pancreas. *Mechanisms of development* **126**, 687-699, doi:10.1016/j.mod.2009.05.005 (2009).

36 Jensen, J. *et al.* Independent development of pancreatic alpha- and beta-cells from neurogenin3-expressing precursors: a role for the notch pathway in repression of premature differentiation. *Diabetes* **49**, 163-176 (2000).

37 Liu, Z. *et al.* Second-generation Notch1 activity-trap mouse line (N1IP::CreHI) provides a more comprehensive map of cells experiencing Notch1 activity. *Development* **142**, 1193-1202, doi:10.1242/dev.119529 (2015).

38 Xue, Y. *et al.* Embryonic lethality and vascular defects in mice lacking the Notch ligand Jagged1. *Hum Mol Genet* **8**, 723-730 (1999).

39 Itoh, M. *et al.* Mind bomb is a ubiquitin ligase that is essential for efficient activation of Notch signaling by Delta. *Dev Cell* **4**, 67-82 (2003).

40 Koo, B. K. *et al.* Mind bomb 1 is essential for generating functional Notch ligands to activate Notch. *Development* **132**, 3459-3470, doi:10.1242/dev.01922 (2005).

41 Koo, B. K. *et al.* An obligatory role of mind bomb-1 in notch signaling of mammalian development. *PLoS One* **2**, e1221, doi:10.1371/journal.pone.0001221 (2007).

42 Villasenor, A., Chong, D. C., Henkemeyer, M. & Cleaver, O. Epithelial dynamics of pancreatic branching morphogenesis. *Development* **137**, 4295-4305, doi:10.1242/dev.052993 (2010).

43 Nishikawa, Y. *et al.* Hes1 plays an essential role in Kras-driven pancreatic tumorigenesis. *Oncogene*, doi:10.1038/s41388-019-0718-5 (2019).

44 Fujikura, J. *et al.* Notch/Rbp-j signaling prevents premature endocrine and ductal cell differentiation in the pancreas. *Cell Metab* **3**, 59-65, doi:10.1016/j.cmet.2005.12.005 (2006).

45 Fujikura, J. *et al.* Rbp-j regulates expansion of pancreatic epithelial cells and their differentiation into exocrine cells during mouse development. *Dev Dyn* **236**, 2779-2791, doi:10.1002/dvdy.21310 (2007).

46 Shimojo, H., Ohtsuka, T. & Kageyama, R. Oscillations in notch signaling regulate maintenance of neural progenitors. *Neuron* **58**, 52-64, doi:10.1016/j.neuron.2008.02.014 (2008).

47 Shimojo, H. & Kageyama, R. Oscillatory control of Delta-like1 in somitogenesis and neurogenesis: A unified model for different oscillatory dynamics. *Semin Cell Dev Biol* **49**, 76-82, doi:10.1016/j.semcdb.2016.01.017 (2016).

48 Sprinzak, D. *et al.* Cis-interactions between Notch and Delta generate mutually exclusive signalling states. *Nature* **465**, 86-90, doi:10.1038/nature08959 (2010).

49 Cras-Meneur, C., Li, L., Kopan, R. & Permutt, M. A. Presenilins, Notch dose control the fate of pancreatic endocrine progenitors during a narrow developmental window. *Genes Dev* **23**, 2088-2101, doi:10.1101/gad.1800209 (2009).

50 Bray, S. & Bernard, F. Notch targets and their regulation. *Curr Top Dev Biol* **92**, 253-275, doi:10.1016/S0070-2153(10)92008-5 (2010).

51 Svensson, P., Bergqvist, I., Norlin, S. & Edlund, H. MFng is dispensable for mouse pancreas development and function. *Mol Cell Biol* **29**, 2129-2138, doi:10.1128/MCB.01644-08 (2009).

52 Dale, J. K. *et al.* Periodic notch inhibition by lunatic fringe underlies the chick segmentation clock. *Nature* **421**, 275-278, doi:10.1038/nature01244 (2003).

53 LeBon, L., Lee, T. V., Sprinzak, D., Jafar-Nejad, H. & Elowitz, M. B. Fringe proteins modulate Notch-ligand cis and trans interactions to specify signaling states. *Elife* **3**, e02950, doi:10.7554/eLife.02950 (2014).

54 Srinivas, S. *et al.* Cre reporter strains produced by targeted insertion of EYFP and ECFP into the ROSA26 locus. *BMC Dev Biol* **1**, 4 (2001).

55 Madisen, L. *et al.* A robust and high-throughput Cre reporting and characterization system for the whole mouse brain. *Nat Neurosci* **13**, 133-140, doi:10.1038/nn.2467 (2010).

56 Hrabe de Angelis, M., McIntyre, J., 2nd & Gossler, A. Maintenance of somite borders in mice requires the Delta homologue DII1. *Nature* **386**, 717-721, doi:10.1038/386717a0 (1997).

57 Kiernan, A. E., Xu, J. & Gridley, T. The Notch ligand JAG1 is required for sensory progenitor development in the mammalian inner ear. *PLoS Genet* **2**, e4, doi:10.1371/journal.pgen.0020004 (2006).

58 Ishibashi, M. *et al.* Targeted disruption of mammalian hairy and Enhancer of split homolog-1 (HES-1) leads to up-regulation of neural helix-loop-helix factors, premature neurogenesis, and severe neural tube defects. *Genes Dev* **9**, 3136-3148 (1995).

59 Engert, S., Liao, W. P., Burtscher, I. & Lickert, H. Sox17-2A-iCre: a knock-in mouse line expressing Cre recombinase in endoderm and vascular endothelial cells. *Genesis* **47**, 603-610, doi:10.1002/dvg.20540 (2009).

60 Kawaguchi, Y. *et al.* The role of the transcriptional regulator Ptf1a in converting intestinal to pancreatic progenitors. *Nat Genet* **32**, 128-134, doi:10.1038/ng959 (2002).

61 Choi, E. *et al.* Dual lineage-specific expression of Sox17 during mouse embryogenesis. *Stem cells (Dayton, Ohio)* **30**, 2297-2308, doi:10.1002/stem.1192 (2012).

62 Kanki, H., Suzuki, H. & Itohara, S. High-efficiency CAG-FLPe deleter mice in C57BL/6J background. *Exp Anim* **55**, 137-141 (2006).

63 Ahnfelt-Ronne, J. *et al.* An improved method for three-dimensional reconstruction of protein expression patterns in intact mouse and chicken embryos and organs. *J Histochem Cytochem* **55**, 925-930, doi:10.1369/jhc.7A7226.2007 (2007).

64 Johnston, S. H. *et al.* A family of mammalian Fringe genes implicated in boundary determination and the Notch pathway. *Development* **124**, 2245-2254 (1997).

65 Burgess, A. *et al.* Loss of human Greatwall results in G2 arrest and multiple mitotic defects due to deregulation of the cyclin B-Cdc2/PP2A balance. *Proc Natl Acad Sci U S A* **107**, 12564-12569, doi:10.1073/pnas.0914191107 (2010).

66 McCloy, R. A. *et al.* Partial inhibition of Cdk1 in G 2 phase overrides the SAC and decouples mitotic events. *Cell Cycle* **13**, 1400-1412, doi:10.4161/cc.28401 (2014).

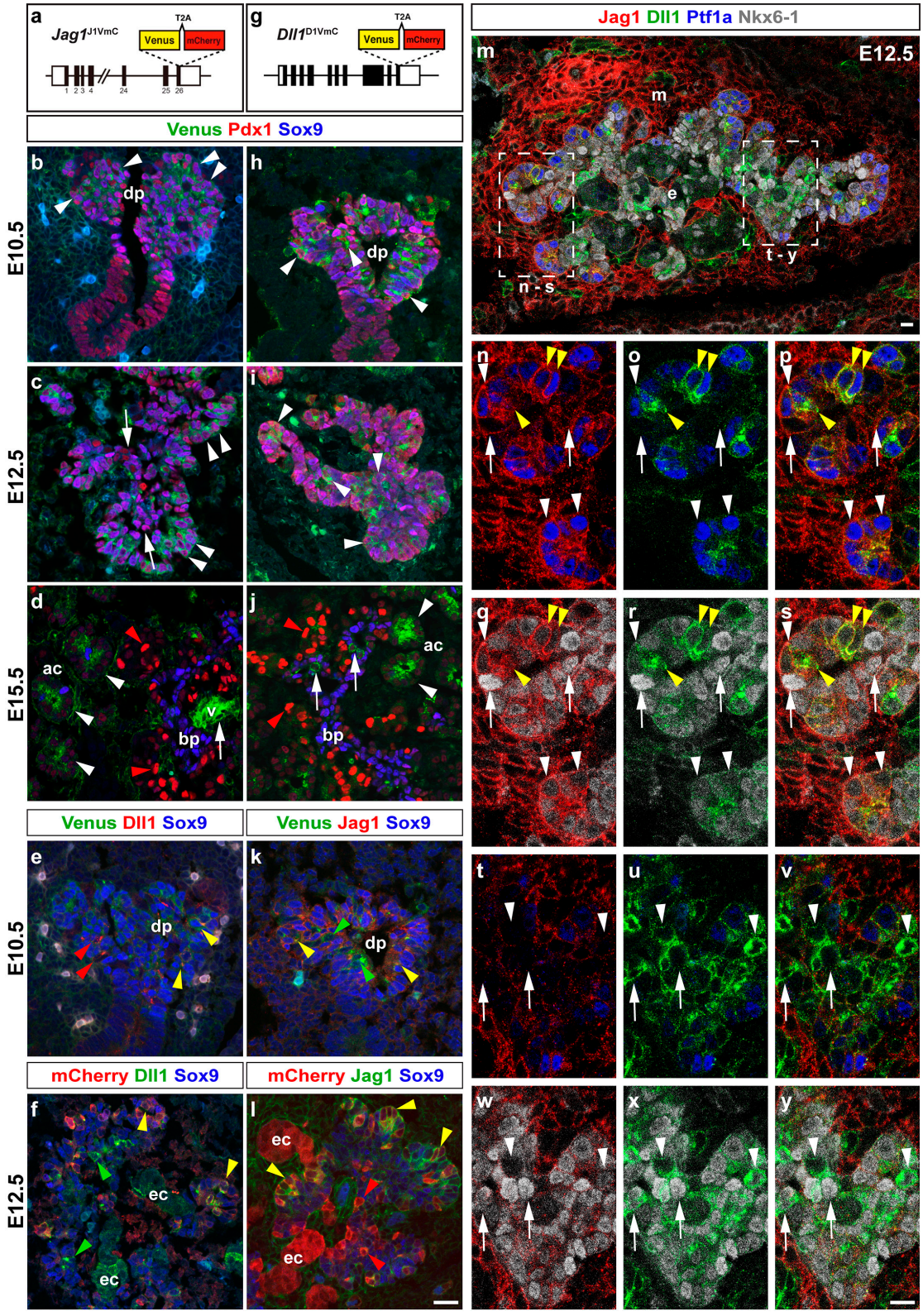

Figure 1

Fig. 1. Nascent PACs co-express Jag1 and Dll1. **a**, **g** Schematics of the *Jag1*^{J1VmC} **a** and *Dll1*^{D1VmC} **g** fusion protein reporters. **b**-**f** Sections of E10.5 **b**, **e**, E12.5 **c**, **f** and E15.5 **d** *Jag1*^{J1VmC} embryos stained for Jag1-Venus, Pdx1 and Sox9 **b**-**d**, Jag1-Venus, Dll1 and

Sox9 **e**, or Jag1-mCherry, Dll1 and Sox9 **f**, as indicated. **h**-**l** Sections of E10.5 **h**, **k**, E12.5 **i**, **l** and E15.5 **j** *Dll1*^{D1VmC} embryos stained for Dll1-Venus, Pdx1 and Sox9 **h**-**j**, Dll1-Venus, Jag1 and Sox9 **k**, or Dll1-mCherry, Jag1 and Sox9 **l**, as indicated. Note uniform Jag1-Venus expression in E10.5 MPCs (arrowheads in **b**), confined to distal epithelium at E12.5 (arrowheads in **c**) and absent from central epithelium (arrows in **c**), and to vessels (arrow in **d**) and acini (arrowheads in **d**) at E15.5. dp: dorsal pancreas; ac: forming acini; bp: bi-potent progenitors; v: vasculature. In contrast, Dll1-Venus expression is seen scattered cells in E10.5 and E12.5 central and distal epithelium (arrowheads in **h** and **i**) and in E15.5 acini (arrowheads in **j**) and scattered cells in the central epithelium (arrows in **j**). **e**, **k** some E10.5 MPCs (Sox9^{+}) co-express Jag1 and Dll1 (yellow arrowheads in **e** and **k**) while scarce Jag1^{-}Dll1^{+} cells (red and green arrowheads in **e** and **k**, respectively) likely represent endocrine precursors (Sox9$^{Lo/-}$). **f**, **l** nascent PACs (Sox9 $^{Lo/-}$) co-express Jag1 and Dll1 at E12.5 (yellow arrowheads in **f** and **l**) while scarce Jag1^{-}Dll1^{+} cells (green and red arrowheads in **f** and **l**, respectively) likely represent endocrine precursors (Sox9$^{Lo/-}$). Note endocrine clusters (ec) are Dll1^{+}. **m** Section of E12.5 wild type embryo containing the dorsal pancreas stained for Jag1 (red), Dll1 (green), Ptf1a (blue) and Nkx6-1 (grey). **n**-**y** Magnifications of boxed fields in **m** with various channels omitted for clarity. **n**-**s** Note Jag1^{Hi}Dll1^{Hi} (yellow arrowheads) as well as Jag1^{Hi}Dll1^{Lo} (white arrowheads in **n**-**s**) cells among the Ptf1a^{+}Nkx6-1^{-} cells, while Nkx6-1^{Hi} cells (arrows) are Ptf1a^{-}Jag1^{Lo}Dll1$^{Lo/-}$. **t**-**y** Note Dll1^{+} cells in the trunk epithelium are Jag1^{-}. Some of these are Nkx6-1^{+} (arrows) and some are Nkx6-1^{-} (arrowheads). m: mesenchyme; e: epithelium. Scale bars 20 μm **b**-**f**,**h**-**l** and 10 μm **m**-**y**.

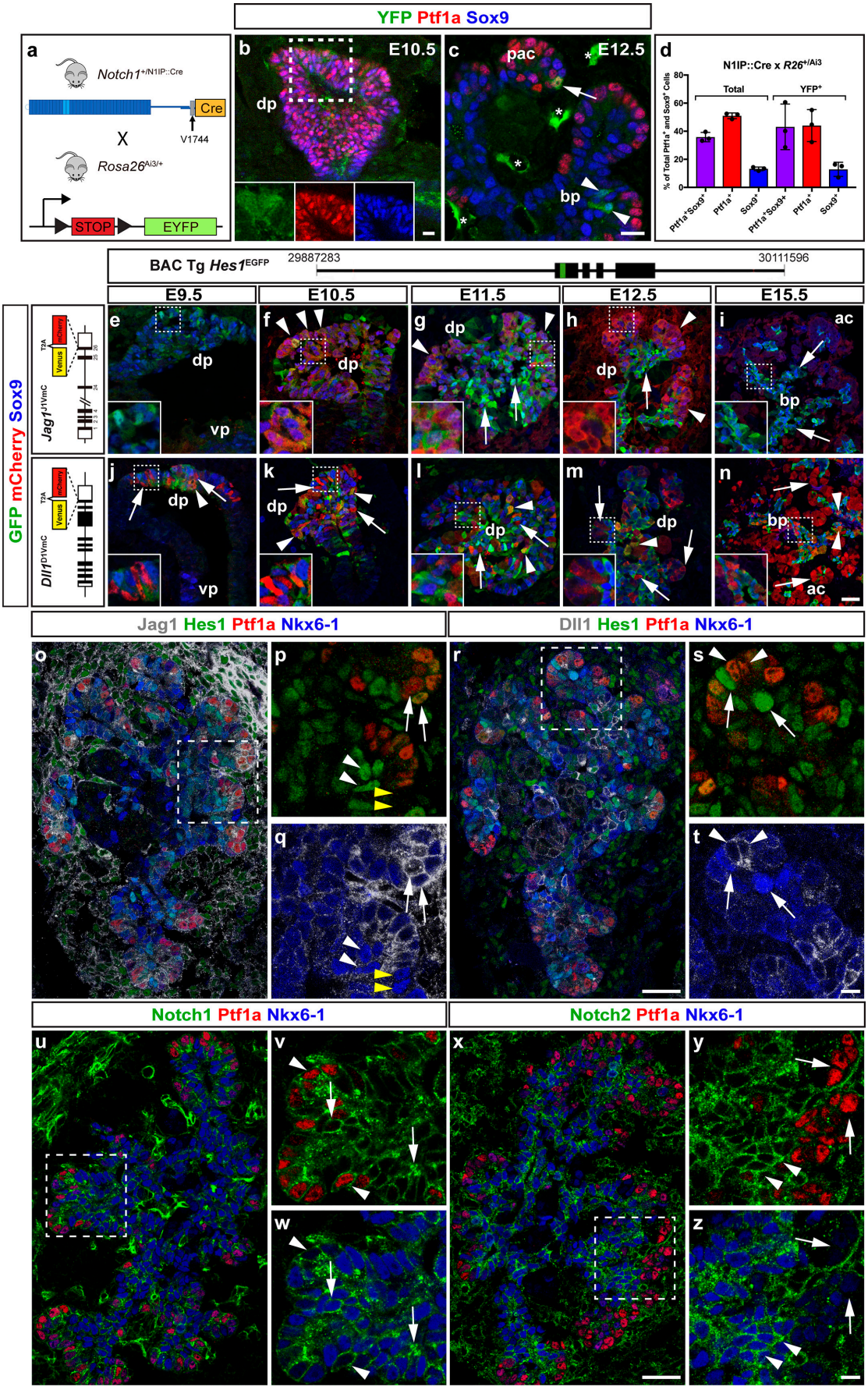

Figure 2

Fig. 2. Notch activation is attenuated in nascent PACs. **a** Schematic showing lineage-tracing setup using N1IP::Cre to label cells with a history of Notch1 activation. **b**, **c** Sections of E10.5 **b** and E12.5 **c** dorsal pancreas from an N1IP::Cre; Rosa26$^{Ai3/+}$ embryo stained for YFP, Ptf1a and Sox9 as indicated. Insets show individual channels for clarity. Note YFP-labeled, E12.5 epithelial cells can be either Sox9^{+} (arrowheads) or Ptf1a^{+} (arrow). Endothelial cells are indicated by asterisks. **d** Bar graph/scatter plot showing quantification of YFP-labeled versus unlabeled epithelial cells expressing Sox9, Ptf1a, or both. Mean ± S.D. is shown; N=3 embryos. There is no significant enrichment of labeled cells with any marker combination tested. **e-i** Sections of E9.5 **e**, E10.5 **f**, E11.5 **g**, E12.5 **h** and E15.5 **i** *Jag1*^{J1VmC} embryos stained for Jag1-mCherry, Hes1-GFP, and Sox9 as indicated. **j-n** Sections of E9.5 **j**, E10.5 **k**, E11.5 **l**, E12.5 **m** and E15.5 **n** *Dll1*^{D1VmC} embryos stained for Jag1-mCherry, Hes1-GFP, and Sox9 as indicated. Note that Jag1-mCherry and Hes1-GFP initially are co-expressed in most Sox9^{+} progenitor cells (arrowheads in **f**) but that Jag1-mCherry segregates to distal cells through E11.5 and E12.5 (arrowheads in **g** and **h**) while Hes1-GFP segregates to proximal cells (arrows in **g** and **h**). **i** By E15.5 Sox9^{+} BPs are Hes1-GFP^{+} and Jag1-mCherry^{-} (arrows). Note that Dll1-mCherry is heterogeneously expressed during early development (arrowheads in **j**-**m**). Dll1-mCherry is frequently co-expressed with Hes1-GFP in early MPCs (arrowheads in **j** and **k**) and later in the proximal bp region (arrowheads in **l**-**n**). Dll1-mCherry single positive cells (arrows in **j**-**n**) segregate to the distal region through development. dp: dorsal pancreas; vp: ventral pancreas; bp: bi-potent progenitor domain; ac: emerging acini. **o-t** Serial sections of E12.5 dorsal pancreas stained for Ptf1a, Nkx6-1, Hes1 and either Jag1 **o-q** or Dll1 **r-t**, as indicated. **p**, **q** Nkx6-1^{+} cells can be either Hes1^{+} (white arrowheads) or Hes1^{-} (yellow arrowheads), while Ptf1a^{+} cells are Jag1^{+}Nkx6-1$^{Lo/-}$ (arrows). **s**, **t** Nhx6-1^{Hi}Hes1^{Hi} cells in distal epithelium (arrows) are adjacent to Ptf1a^{+}Dll1^{Hi} cells (arrowheads). **u-z** Serial sections of E12.5 dorsal pancreas stained for Ptf1a, Nkx6-1, and either Notch1 **u-w** or Notch2 **x-z**, as indicated. **u-w** Notch1 is expressed in both Ptf1a^{+} cells (arrowheads) and Nkx6-1^{+} cells (arrows). **x-z** Notch2 is expressed in Nkx6-1^{+} cells (arrowheads) but not in Ptf1a^{+} cells (arrows).

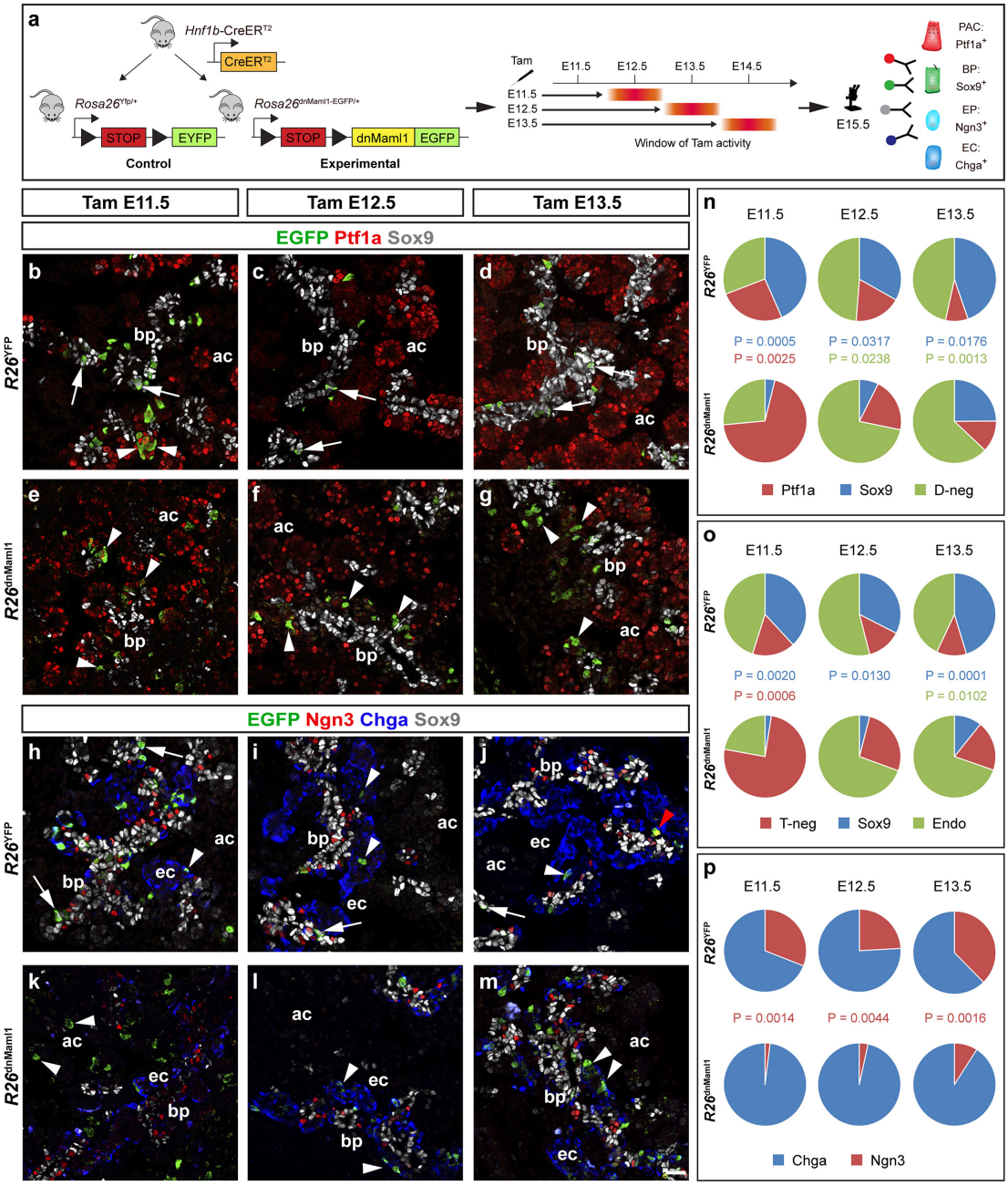

Figure 3

Fig. 3. Stage-dependent allocation of progenitor fate induced by Notch suppression. **a** Schematic overview of strategy applied to identify fates of progeny from pancreatic progenitors in which Notch-mediated transcriptional activation is prevented by *Hnf1b-CreER*^{T2}-mediated expression of a dnMaml1-GFP fusion protein from the *Rosa26* locus at different developmental stages. Approximate temporal windows of Tamoxifen (Tam) activity resulting from single intraperitoneal injections at E11.5, E12.5 or E13.5 and cell fate-specific markers are indicated. PAC: pre-acinar cells; BP: bipotent progenitors; EP: endocrine precursors; EC: endocrine cells. **b**-**m** Sections of

E15.5 *Hnf1b-CreER^{T2}*; *R26^{YFP}* control **b**-**d**, **h**-**j** or *Hnf1b-CreER^{T2}*; *R26^{dnMaml1}* Notch-blocked **e**-**g**, **k**-**m** pancreata stained for EYFP/EGFP and Sox9 combined with either Ptf1a **b**-**g** or Ngn3 and Chga **h**-**m**, as indicated. bp: bi-potent progenitor domain; ac: emerging acini; ec: endocrine cells. Scale bar 50 μm. **b**-**g** Note lineage-labeled Sox9$^+$ BPs (arrows in **b**-**d**) and Ptf1a$^+$ PACs (arrowheads in **b**) in control panels (*R26^{YFP}*) and lineage-labeled Ptf1a$^+$ PACs (arrowheads in **e**) and Ptf1a/Sox9 double negative cells (arrowheads in **f** and **g**) in experimental panels (*R26^{dnMaml1}*). **h**-**m** Note lineage-labelled Sox9$^+$ BPs (arrows in **h**-**j**), Chga$^+$ endocrine cells (arrowheads in **i** and **j**), and a Ngn3$^+$ endocrine precursor (red arrowhead in **j**) in control panels (*R26^{YFP}*) and lineage-labeled Ngn3/Chga/Sox9 triple negative cells (arrowheads in **k**) and Chga$^+$ endocrine cells (arrowheads in **l** and **m**) in experimental panels (*R26^{dnMaml1}*). **n**, **o** Quantification of *R26^{YFP}*- *versus* *R26^{dnMaml1}* (EGFP)-labeled cell distribution at E15.5 following Tam administration at E11.5, E12.5 or E13.5 as indicated. Pie charts show fractions of EYFP/EGFP-labeled cells expressing Ptf1a, Sox9 or neither marker (D-neg) **n**; or Sox9, endocrine markers (Endo, Ngn3+Chga) or none of the three (T-neg) **o**. **p** Pie chart showing the proportions of labeled cells in the endocrine lineage expressing either Ngn3 or Chga. Significant changes in allocation to distinct cell fates between *R26^{dnMaml1}* and controls are indicated by font color **n**-**p**.

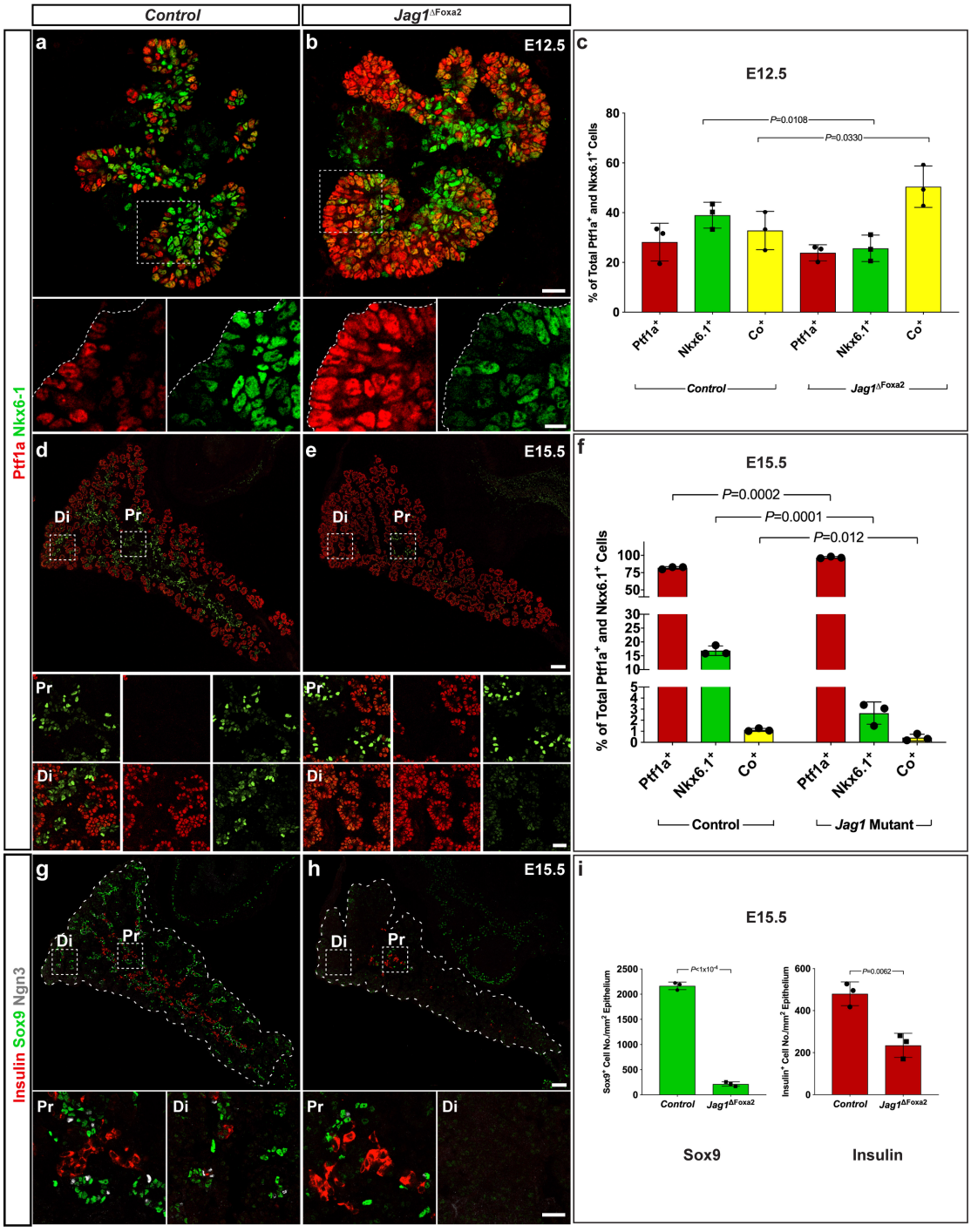

Fig. 4. Extensive loss of BPs and their progeny in *Jag1*$^{\Delta Foxa2}$ pancreas. **a**-**b** IF for Ptf1a and Nkx6-1 as indicated on E12.5 dorsal pancreas from control **a** and *Jag1*$^{\Delta Foxa2}$ **b** embryos. Note that Ptf1a expression extends more proximally within the *Jag1*$^{\Delta Foxa2}$ pancreas (insets in **a** and **b**). **c** Increased proportion of Ptf1a^{+}Nkx6-1^{+} double-positive cells at the expense of Nkx6-1^{+} single-positive BPs in the E12.5 *Jag1*$^{\Delta Foxa2}$ pancreas. **d**, **e** IF for Ptf1a and Nkx6-1 as indicated reveals loss of Nkx6-1^{+} cells in E15.5 *Jag1*$^{\Delta Foxa2}$ mutants **e** relative to control littermates **d**. Insets in **d** and **e** show that distal (Di) Nkx6-

1^+ cells are entirely eliminated while some of the proximal-most (Pr) Nkx6-1^+ cells being retained in the *Jag1*$^{\Delta Foxa2}$ pancreas. **f** Quantitatively, ~85% of the Nkx6-1^+ cells are lost on average while Ptf1a$^+$ are proportionally increased in E15.5 *Jag1*$^{\Delta Foxa2}$ compared to controls. **g**, **h** IF for Sox9, Ngn3 and insulin as indicated reveals loss of Sox9$^+$ BPs and BP-derived, Ngn3$^+$ endocrine precursors and insulin$^+$ β-cells. Insets in **g**, **h** show that similar to Nkx6-1^+ cells, the distal (Di) Sox9$^+$ cells are completely lost in *Jag1*$^{\Delta Foxa2}$ pancreas: only a small fraction of the proximal-most (Pr) Sox9$^+$ cells are retained. **i** Quantitatively, BPs and β-cells are reduced by ~90% and ~50%, respectively, in E15.5 *Jag1*$^{\Delta Foxa2}$ compared to control littermates. Scale bars, 100 μm (main panels) and 25 μm (insets).

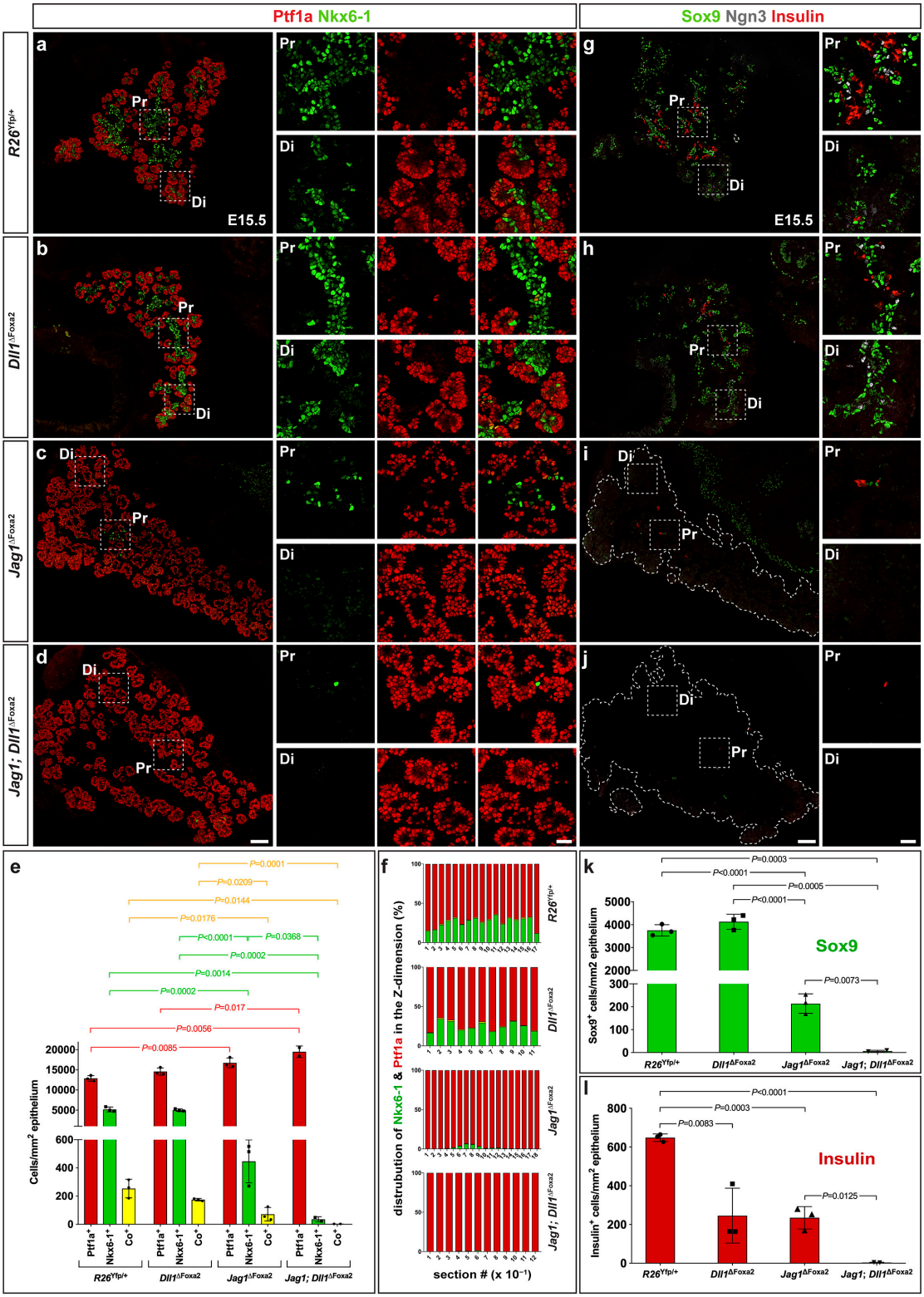

Figure 5

Fig. 5. Complete conversion of progenitors into PACs in *Jag1-Dll1* double mutant mice. **a**-**d** IF for Ptf1a and Nkx6-1 as indicated on sections of E15.5 *wild-type* **a**, *Dll1*$^{\Delta Foxa2}$ **b**, *Jag1*$^{\Delta Foxa2}$ **c**, and *Jag1*; *Dll1*$^{\Delta Foxa2}$ **d** mutant dorsal pancreata. Di: distal; Pr: proximal. Scale bars, 100 μm and 25 μm in insets. **e** Quantitative analyses reveals no change in

the ratio of Ptf1a$^+$, Nkx6-1$^+$ or Ptf1a$^+$Nkx6-1$^+$ (Co$^+$) cells between *Dll1*$^{\Delta Foxa2}$ and *R26*^{YFP} control pancreata at E15.5 while Nkx6-1$^+$ cells are severely depleted in *Jag1*$^{\Delta Foxa2}$ mutants with a concordant increase in Ptf1a$^+$ cells. Compound *Jag1*; *Dll1*$^{\Delta Foxa2}$ mutants exhibit a more profound loss of Nkx6-1$^+$ cells and gain of Ptf1a$^+$ cells than either single mutant. Insets in **c**, **d** show that residual Nkx6-1$^+$ cells were confined to the proximal-most core of both single *Jag1*$^{\Delta Foxa2}$ mutants and compound *Jag1*; *Dll1*$^{\Delta Foxa2}$ mutants. **f** Distribution of Nkx6-1$^+$ cells on every 10th section in the *z*-dimension is shown. The data confirms confinement to the core of the organ in both single *Jag1*$^{\Delta Foxa2}$ mutants and compound *Jag1*; *Dll1*$^{\Delta Foxa2}$ mutants. **g**-**j** IF for Sox9, Ngn3 and insulin as indicated on sections of E15.5 pancreata reveals Sox9$^+$ cell numbers to be unchanged between E15.5 *Dll1*$^{\Delta Foxa2}$ and *R26*^{YFP} control pancreata while they are severely reduced in *Jag1*$^{\Delta Foxa2}$ mutants and compound *Jag1*; *Dll1*$^{\Delta Foxa2}$ mutants. Di: distal; Pr: proximal. Scale bars, 100 μm and 25 μm in insets. **k** Quantitative analysis revealed a ~90% loss of Sox9$^+$ cells in *Jag1*$^{\Delta Foxa2}$ mutants and a 99.7% reduction in *Jag1*; *Dll1*$^{\Delta Foxa2}$ mutants. **l** The number of insulin$^+$ β-cells are reduced in both E15.5 *Dll1*$^{\Delta Foxa2}$ and *Jag1*$^{\Delta Foxa2}$ mutants relative to *R26*^{YFP} controls while compound *Jag1*; *Dll1*$^{\Delta Foxa2}$ mutants lost essentially all β-cells.

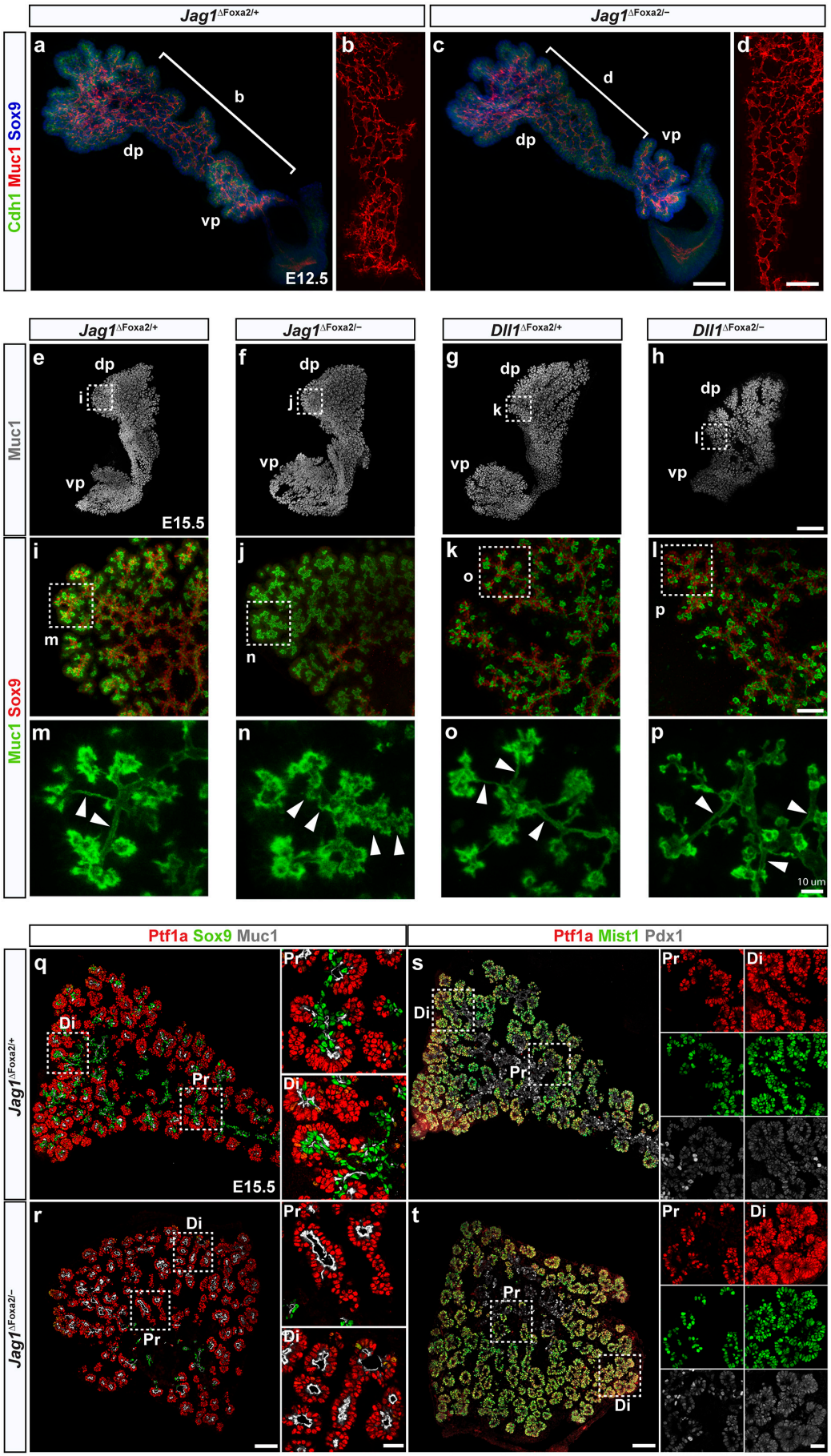

Figure 6

Fig. 6. Normal plexus formation and organ architecture in *Jag1*$^{\Delta Foxa2}$ mutants. **a**, **c** 3D maximum intensity projections (MIP) of the midgut region of E12.5 *Jag1*$^{\Delta Foxa2/+}$ and *Jag1*$^{\Delta Foxa2/-}$ embryos stained for Cdh1, Muc1 and Sox9 as indicated by whole-mount IF. White brackets indicate regions shown in **b** and **d**. Note the normal organ architecture and plexus formation. Scale bar, 50 µm. **b**, **d** Higher magnification of the body region of dorsal pancreata showing only the Muc1 staining to emphasize the luminal plexus. Scale bar, 25 µm. **e**-**h** 3D MIP of whole-mount, Muc1 labeled E15.5 *Jag1*$^{\Delta Foxa2/+}$ **e**, *Jag1*$^{\Delta Foxa2/-}$ **f**, *Dll1*$^{\Delta Foxa2/+}$ **g**, and *Dll1*$^{\Delta Foxa2/-}$ **h** pancreata. Note normal organ architecture in *Jag1*$^{\Delta Foxa2/-}$ mutants while *Dll1*$^{\Delta Foxa2/-}$ mutants show a truncated pancreas with the head and body more severely affected than the tail. Scale bar, 300 µm. **i**-**l** Higher power images of maximum intensity projections from sub-stacks acquired from the boxed areas indicated in **e**-**h** showing Muc1 and Sox9 distribution. Note the tree-like organization of the terminal ducts in all genotypes. Scale bar, 50 µm. **m**-**p** Higher power images of boxed areas indicated in **i**-**l** showing Muc1 alone to emphasize the structure of the terminal ducts. Note the serrated appearance of terminal duct lumens in *Jag1*$^{\Delta Foxa2/-}$ mutants while heterozygote littermate controls and *Dll1*$^{\Delta Foxa2/-}$ mutants show smooth lumens (arrowheads in **m**-**p**). Scale bar, 10 µm. **q**-**t** Sections of E15.5 *Jag1*$^{\Delta Foxa2/+}$ **q**, **s** and *Jag1*$^{\Delta Foxa2/-}$ **r**, **t** pancreata stained for Ptf1a (red), Sox9 (green) and Muc1 (grey) **q**, **r** or Ptf1a (red), Mist1 (green) and Pdx1 (grey) **s**, **t**. Note that Sox9^{+} terminal duct cells connecting to acini in controls are replaced by Ptf1a^{+}Mist1^{+} elongated "duct"-like structures in *Jag1*$^{\Delta Foxa2/-}$ mutants in both proximal (Pr) and distal (Di) regions (insets show boxed areas in higher magnification). Scale bars, 100 µm (main panels) and 25 µm (insets).

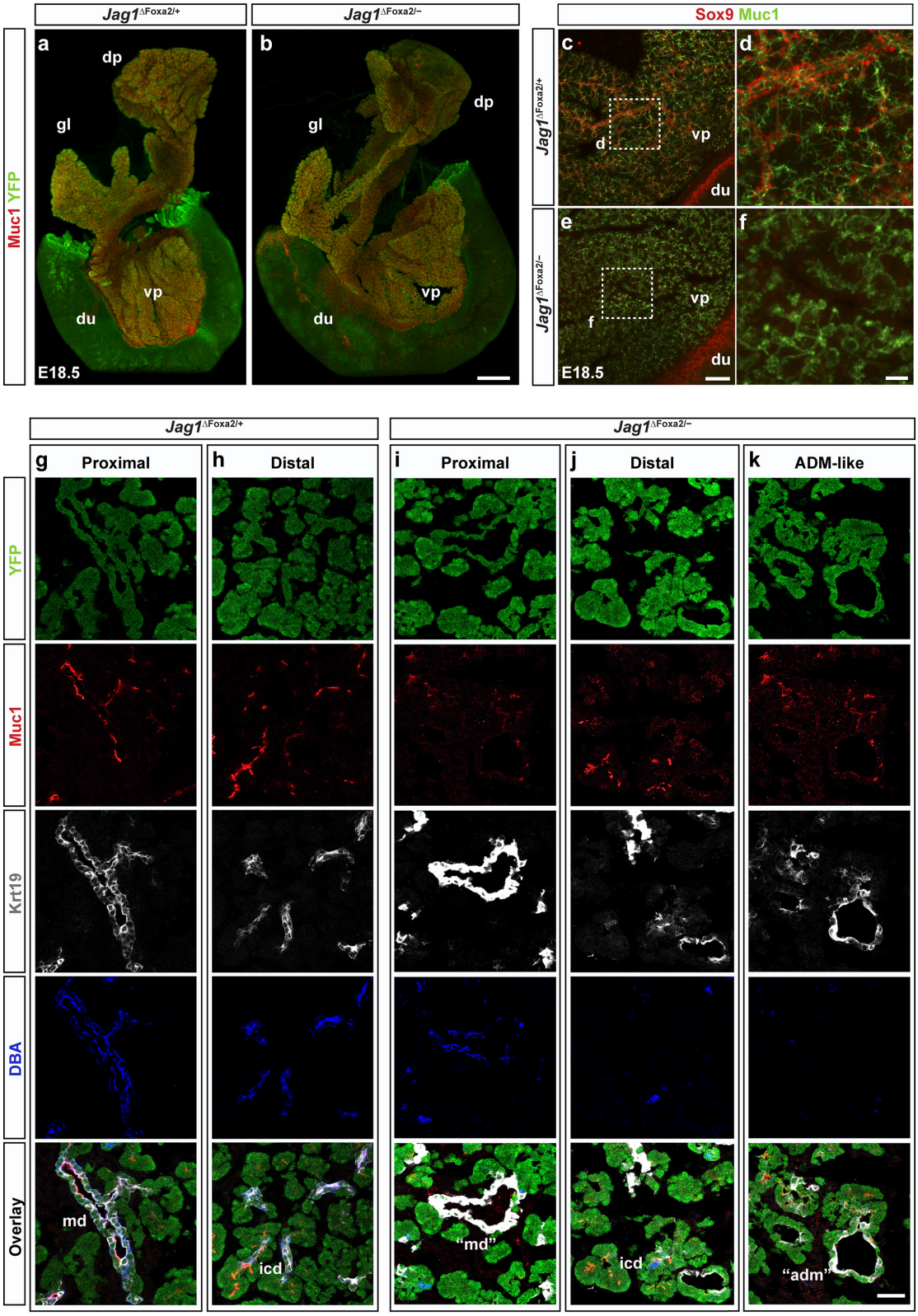

Figure 7

Fig. 7. Ductal malformations and signs of acinar-to-ductal metaplasia in E18.5 *Jag1*$^{\Delta Foxa2}$ embryos. **a**-**f** 3D maximum intensity projections of E18.5 *Jag1*$^{\Delta Foxa2/+}$ and *Jag1*$^{\Delta Foxa2/-}$ whole-mount pancreata stained for Muc1 and YFP as indicated. **a**, **b** low

magnification overview showing normal overall organ architecture with clearly delineated dorsal pancreas (dp), gastric lobe (gl) and ventral pancreas (vp) in the loop of the duodenum (du) in E18.5 *Jag1*$^{\Delta Foxa2/-}$ mutants relative to *Jag1*$^{\Delta Foxa2/+}$ littermates. Scale bar, 700 µm. **c**-**f** Higher power images show both interlobular and large intralobular ducts to be completely absent in *Jag1*$^{\Delta Foxa2/-}$ mutants compared to controls (boxed areas in **c** and **e** are shown at higher power in **d** and **f**, respectively). Scale bars, 100 µm in **c**, **e** and 25 µm **d**, **f**. **g**-**k** High magnification views of E18.5 *Jag1*$^{\Delta Foxa2/+}$ **g**, **h** and *Jag1*$^{\Delta Foxa2/-}$ **i**-**k** pancreata stained for YFP, Muc1, Krt19 and DBA as indicated (see Supplementary Fig. 9a, b for low magnification views). Note the general paucity of the ductal tree, disrupted main duct (md), abnormal morphology of intercalated ducts (icd) and dilated epithelial (YFP$^+$) Krt19$^+$DBA$^-$ ADM-like structures with little to no Muc1 ("adm") in the *Jag1*$^{\Delta Foxa2/-}$ pancreas **i**-**k** resembling those seen in acinar-to-ductal metaplasia **k**. Scale bar, 25 µm.

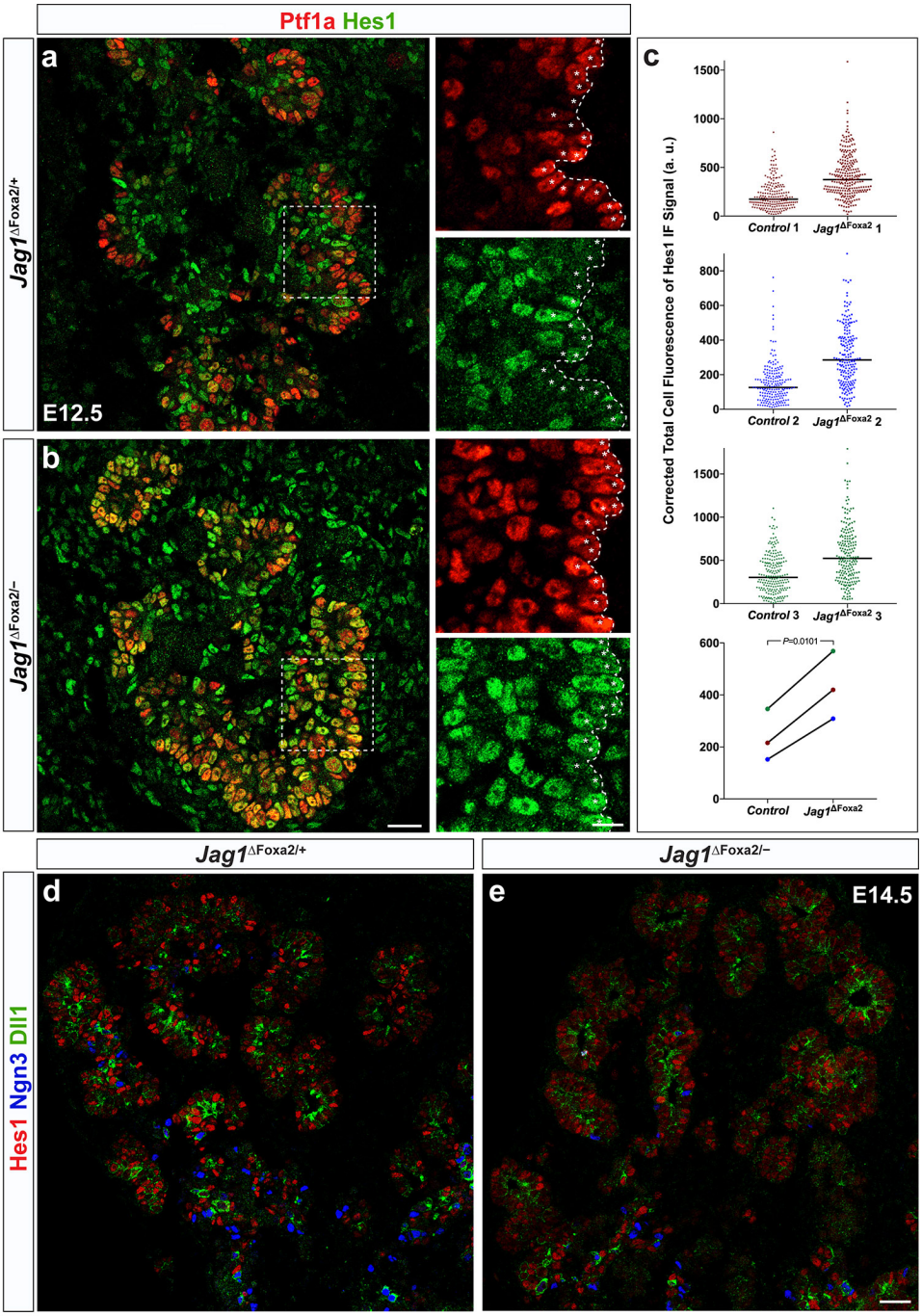

Figure 8

Fig. 8. Prolonged MPC state of *Jag1*$^{\Delta Foxa2}$ mutants is coupled to increased Notch activity. **a, b** Sections of E12.5 *Jag1*$^{\Delta Foxa2/+}$ **a** and *Jag1*$^{\Delta Foxa2/-}$ **b** pancreata stained for Ptf1a (red) and Hes1 (green). Note that Ptf1a marks only the distal-most epithelial cells (PACs) in *Jag1*$^{\Delta Foxa2/+}$ pancreas, while being expressed more proximally within the *Jag1*$^{\Delta Foxa2/-}$ pancreas. Also note that Hes1 is upregulated, particularly in the distal Ptf1a^{+} PACs (asterisks) in *Jag1*$^{\Delta Foxa2/-}$ mutants compared with heterozygote littermate controls. Scale bars, 25 μm (main panels) and 10 μm (insets). **c** Quantification of Hes1

corrected total cell fluorescence (CTCF) signal in distal Ptf1a^{+} cells reveals increased signal in *Jag1*$^{\Delta Foxa2/-}$ mutants relative to controls. Scatter plots show intensity values for individual cells in three mutant-control pairs in three, separate IF experiments. Changes in mean values for each pair of embryos are shown color-coded in the lower plot (a.u., arbitrary units). **d**-**g** Sections of E13.5 **d**, **e** and E14.5 **f**, **g** *Jag1*$^{\Delta Foxa2/+}$ **d**, **f** and *Jag1*$^{\Delta Foxa2/-}$ mutant **e**, **g** pancreata stained for Hes1 (red), Ngn3 (blue) and Dll1 (green). YFP expression from the recombined *R26*^{YFP} locus was used to mask the image to avoid visualization of mesenchymal signals. The increase in Hes1^{Hi} cells seen in E12.5 *Jag1*$^{\Delta Foxa2/-}$ mutant **a**, **b** is no longer evident at E13.5 **d**, **e** and appears decreased at E14.5 relative to controls **f**, **g**. In contrast, Dll1 expression appears similar in control and *Jag1*$^{\Delta Foxa2/-}$ mutant pancreas at both E13.5 and E14.5. Scale bar, 50 µm.

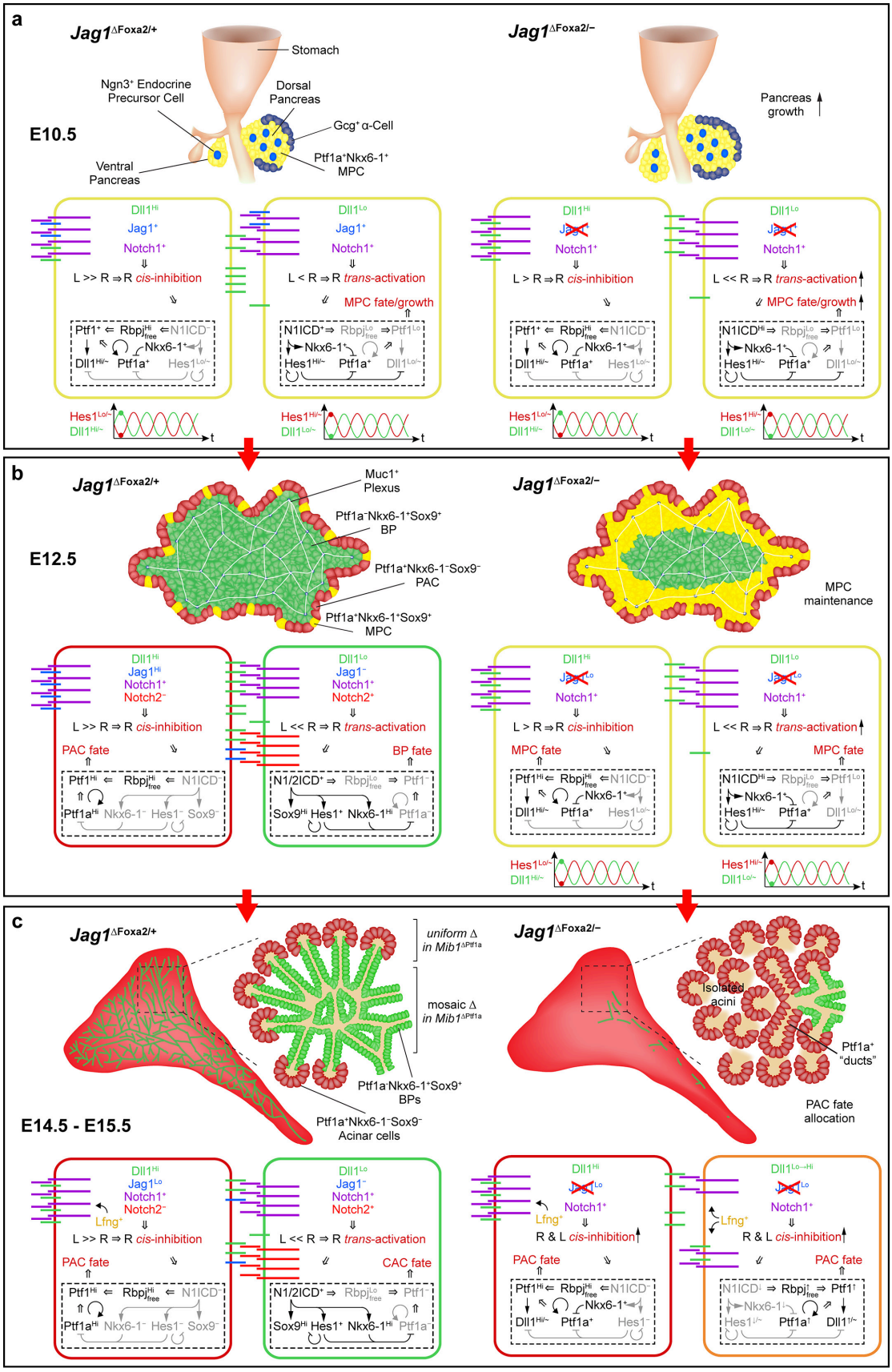

Figure 9

Fig. 9. Proposed model for pancreatic Jag1 function in exit from multipotency and cell fate allocation. **a** Initially, multipotent progenitors (MPCs) proliferate at a given rate, in part determined by input from Notch receptors. High levels of the ligand (L) Dll1 in one cell mediate receptor (R) activation in neighbors resulting in activation of Hes1. A low level of the ligand Jag1 attenuates receptor activation by sequestering a fraction of the receptors (R *cis*-inhibition). The Ptf1a/Rbpj complex (Ptf1) activates *Dll1* expression while Hes1 represses *Dll1* and itself, with the latter likely causing the observed ultradian oscillations of both Hes1 and Dll1. The oscillations enable a temporal symmetry where MPCs alternate between sending and receiving mitogenic input via Notch. Deletion of Jag1 removes its dampening effect on Notch activity resulting in increased MPC proliferation but does affect oscillations. **b** Increased Jag1 expression breaks the symmetry by sequestering all receptors in emerging $Dll1^{Hi}Jag1^{Hi}$ cells pro-acinar cells (PACs) and bolstering free ligand levels. As a result, *trans*-activation is augmented in nascent bi-potent progenitors (BPs), which is further reinforced by onset of Notch2 expression and loss of Jag1-mediated attenuation. Loss of Jag1 prevents symmetry breaking and exit from the multipotent state, except in the central-most progenitors, which receive high Dll1 input from $Ngn3^{+}$ endocrine precursors. **c** Specification of centroacinar cells (CACs) and terminal duct progenitors require Mib1 and Dll1 *or* Jag1 function in PACs. Areas of uniform and mosaic deletion (Δ) in E15.5 $Mib1^{\Delta Ptf1a}$ embryos are indicated. MPCs symmetry is broken and a PAC fate adopted in E14.5 – E15.5 *Jag1* mutants when Notch activation is attenuated, possibly by the onset of Lunatic fringe (Lfng) expression. Hatched boxes show the genetic circuitry (arrows) and protein-protein interactions (double line arrows) underlying the regulatory logic determining cell fate choices. Black indicates active, and grey inactive, components and connections.